MEDWIN PUBLISHERS
Committed to Create Value for Researchers

Petroleum & Petrochemical Engineering Journal
ISSN: 2578-4846

Unique Amphibole-Bearing Mantle Column Beneath the Leningrad Kimberlite Pipe, West Ukukit Field, NE Yakutia

Ashchepkov IV[1,2]*, Babushkina SA[3], Oleinikov OB[3], Medvedev NS[4], Yudin DS[1] and Karmanov NS[1]

[1]Geology, Institute of Geology and Mineralogy SB RAS, Russian Federation
[2]Institute of Geochemistry SB RAS, Russia
[3]Institute of Geology of Diamond and Precious Metals, Siberian Branch, Russian Academy of Sciences, Russia
[4]Nikolaev Institute of Inorganic Chemistry, Russia

Research Article
Volume 7 Issue 2
Received Date: March 27, 2023
Published Date: May 03, 2023
DOI: 10.23880/ppej-16000345

***Corresponding author:** Igor V Ashchepkov, Institute of Geochemistry, Russia, Tel: +799139872605;
Email: Ashchepkov@igm.nsc.ru

Abstract

In the subcratonic lithospheric mantle (SCLM) beneath Leningrad pipe (West Ukukit field), Yakutia garnet thermobarometry allows us to identify seven horizons (paleo subduction slab). Microprobe data for Cr-bearing amphiboles >500 grains from mantle xenoliths and concentrates reveal a broad range of compositions changing from Cr- pargasitic hornblendes to pargasites, edinites, kataforites, K-richterites with increasing pressure determined with new amphibole thermobarometer constructed by the first author The low pressure (LP) Cr-hornblendes and pargasites compiles the high-temperature branch (90-60 mw/m2) from 3.5 GPa to Moho traced by basaltic cumulates. In the middle part of SCLM edinites mark 35 to 40 mw/m2 geotherms. At high pressures kataforites also vary in thermal conditions. Richterites near the lithosphere base trace both low –and high temperature convective branches. The amphiboles reveal divisions into 9 chemical groups. The melts coexistion with amphiboles has concave patters typical for subduction related melts. LP varieties reveal Eu inflection U, Rb, Ba, Sr peaks and deep troughs in HFSE (except Zr), Pb. The pargasites show high U peaks and relativle less HFSE depressions. Encreasing in pressure for edinites, kataforites and richterise are accompanied byrise in U and Zr peak gentling of depressions in Th, Sr, Nb and Hf and less in Nb,Ta, Hf and peak in Zr and also decrease in LREE and REE. Clinopyroxenes and garnets show variable trace element patterns and divisions in groups with the plume and subduction signatures. The contrasting behaviour of Ta and Nb is regulated by the rutile partition coefficients likely for primary eclogites. A subduction and Na and K (siliceous) type of fluids percolated through the mantle with abundant eclogites possibly was accompanied by amphibolization at the different levels through all the mantle column. The plume melts produced hybridism with the mantle metasomatic assembleges which created smoother trace element patterns in reacted minerals, clinopyroxene. The new version of monomineral amphibole thermobarometry is suggested.

Keywords: Kimberlite; Garnet; Amphibole; Clinopyroxene; Chromite Mantle lithosphere; Thermobarometry

Introduction

The northern kimberlite fields in Yakutian kimberlite province (YKP) in Siberia belong mainly to the Early Mesozoic plume activity and mostly are barren in diamonds [1-5]. Several kimberlite pipes like Molokuonamskaya, Leningrad, Ruslovaya, Lorik, Svetlana, Djanga, Aerogeologicheskaya, and Universitetskaya contain diamonds in small amounts [6,7]. However, there are plenty of very rich diamond placers in several areas of the northern part of YKP including Kuoyka, Molodo fields, in Ebelyakh and Prilenie [8]. The sources of these rich placers should be Paleozoic or Precambrian, while the most of pipes in the North of YKP are low Triassic to Cretaceous [4,5] (Figure 1).

The pipe Leningrad is one of the largest of the known pipes in the Northern part of YKP. Leningrad is the first kimberlite body identified in Russia and Yakutia by Zaburdin KS (NIIGA) in 1952 in the riverbed of the Omonos river [9].

The amphiboles are not common in mantle xenoliths in the kimberlites Worldwide. But in Siberiam SCLM, where they were found in the mantle xenoliths of Sytykanskaya Yubileynaya, Komsomolskaya pipes [10-13], in Alakit field [11]. The Ca amphiboles are rather frequent in the relatively low pressure (to 4.0 GPa) xenoliths from Obnazhennaya pipe [14,15] and in Prianabarie [16].

The Leningrad pipe mantle xenoliths amphiboles are more frequent than clinopyroxenes. They cover all the compositiobnal variations of the mantle amphiboles [10-29].

In his paper we introduce new amphybole thermobarometry calibratted to 9 GPa using experimental data [18-24] while published before amphibole barometers are calibrated to 4 GPa [18-20]. We try to solve the questions how the compositionals variations and geochemical features are corresponding to the positions in the mantle column and represent the ages determined for the mica and amphiboles from xenoliths.

The trace element (TRE) geochemistry of the mantle amphiboles is studied only for the shallowest spinel lherzolites in orogenic massifs [25,26], in alkali basalts [27,28] and high-pressure kimberlite xenolith [29].

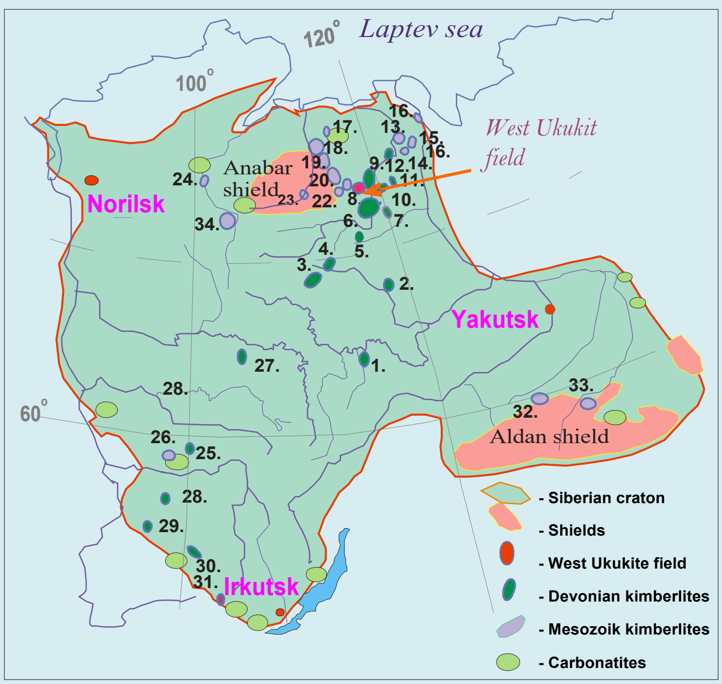

Figure 1: Location of the West Ukukit field and other kimberlite fields in Siberian platform. See legend on the figure. 1. Siberian platform. 2. Shields. Kimberlite fields. 3. West Ukukit field. 4. Late Devonian fields. 5. Lower Triassic and Jurassic fields [1,3]. 6. Carbonatitic massifs. Fields: 1. Malo-Botuobinsky, 2. Nakyn, 3. Alakit-Markha, 4. Daldyn, 5. Upper Muna, 6. Chomurdakh, 7. Severnei, 8. West Ukukit, 9. East Ukukit, 10. Ust-Seligir, 11. Upper Motorchun, 12. Merchimden, 13. Kuoyka, 14. Upper Molodo, 15. Toluop, 16. Khorbusuonka, 17. Ebelyakh, 18. StarayaRechka, 19. Ary-Mastakh, 20. Dyuken, 21. Luchakan, 22. Kuranakh, 23. Middle Koupnamka, 24. Middle Kotui, 25. Chadobets, 26. Taichikun-Nemba, 27. Tychan, 28. Muro-Kova, 29. Tumanshet, 30. Belaya Zima, 31. Ingashi, 32. Chompolo, 33. Tobuk-Khatystyr, 34. Kharamai. 35. Manchary, 36. Carnian tuffs.

In the Leningad kimberlites pipe (West Ukukite filed) amphiboles are frequent both in mantle xenoliths [30,31] and concentratres revealing the very wide range. We determined the positions of the different groups of amphiboles in the mantle columns and suggest the model of their creation. Their formation corresponds to the plume related metasomatism and hybridism with the earlier subduction-related metasomatism.

Geology

Leningrad pipe from West Ukukit field and is one of the largest pipes in the North of Siberia. This field (Figure 2) includes several large pipes Leningrad. Ruslovaya and Omonos in the northern part and Svetlana and Lorik pipes in the south-western part [5]. Most pipes are close to mica-bearing orangeates acccording to estimates of S.A. Babushkina though the main phase of Leningrad pipe contain abundant ilmenites and is tending to common Ca-Mg kimberlite type.

The Leningrad pipe consists of several types of breccia and at least two main intrusive phases [28]. The major phase is autholithic breccia, which contains a huge amount of various xenoliths (Figure 3).

The brightly coloured transparent and well-shaped diamonds were found but in very small amounts <0.01 crt/t and 330 diamond crystals were described [7,29]. The pipe is dated by several methods showing wide variations of ages. The Rb/Sr isochrones on mica and bulk-rock give Devonian age from 380 to 350 Ma with the most probable values ~ 368+-1 Ma [5]. The Ar-Ar for the Phl xenocryst gives 385 Ma [7]. The SHRIMP U/Pb age on zircon, refer to 378 Ma [30]. Thus the age of the Leningrad pipe was suggested as Devonian (368 Ma) and our data on phlogopites also are close (see $^{40}Ar/^{39}Ar$ dating). The earlier ages for the Phl xenocrysts refer most probable to the protokimberlites stage. The pipe Svetlana give similar age 365 Ma as well as several other anomalies. However, some small dykes reveal the younger ages to 350 Ma [5].

But new dating using zircon –U-Pb method give more yonger age 144 Ma [32,33] referring to lates Jurassic kimberlite magmatism in Siberian craton. This may occur because the kimberlites lof this stage are widely spread within the Siberian craton [1,3]. It may occurs that the Leningrad is a complex body compiled by the polysge intrusions.

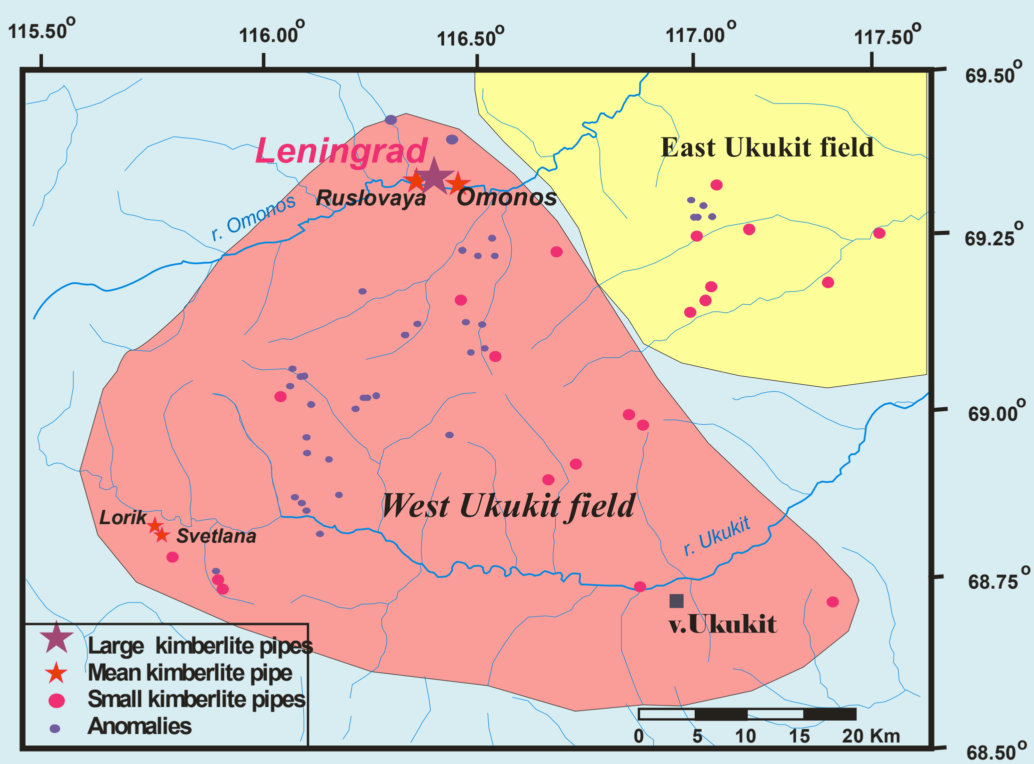

Figure 2: Scheme of the kimberlite pipes location in West Ukukit field. Signs see - figure. Redrawn from [5] with the changes.

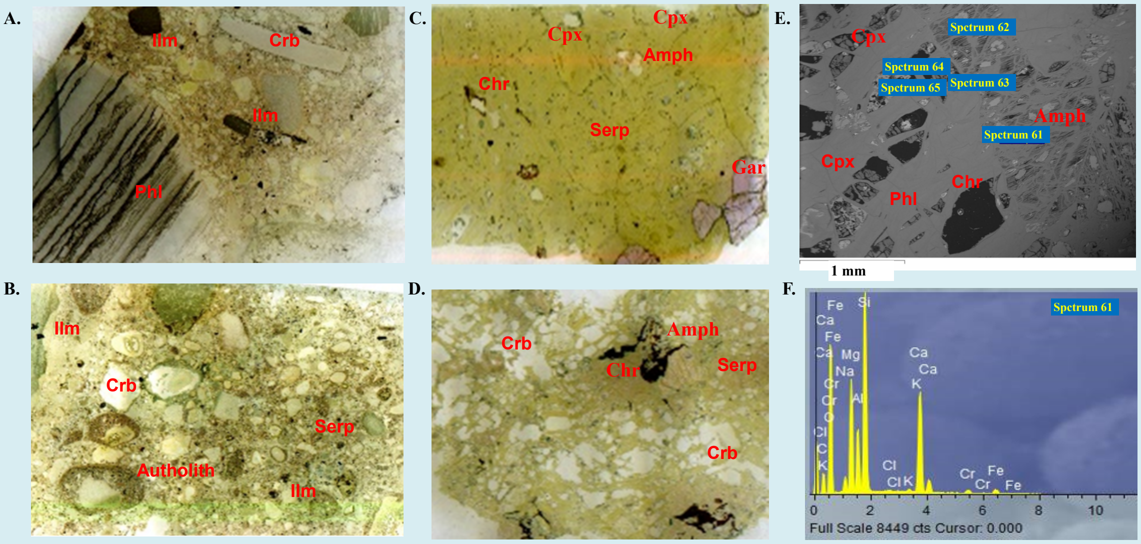

Figure 3: Scanned images of A. Kimberlite from the Leningrad pipe. B. Kimberlite from the Lorik pipe. C. Garnet peridotite xenolith. D. Spinel peridotite with the amphibole and phlogopite. E. Spinel peridotite. F. Spectrum of amphibole. Minerals: Amph- amphibole, Cpx-c inopyroxene. Chr-chromite, Ilm- ilmenite, Carb- carbonate, Serp- serpentine.

Materials and Methods

The pipe was sampled by Oleinnikov OB and Nikishov KN during field works in the 1980th. The samples were preliminarily studied by Babushkina SA using microscopy and electron microprobe analyses (EPMA). They were obtained on partly serpentinized xenoliths and washed concentrates from the kimberlite debris [30-32]. In the thin sections, it is clear that amphiboles are in intergrowth with the Cr-spinels sometimes with the ilmenites and apatites, and Cr- rutiles. The electrone microscope analyses show that they are in interowth and have inclusions of barite and Sr - carbonates as well as various sulfides (Figure 3) (pentlandite, chalcopyrite, pyrrhotite) (see supplementary file 1) (SF1).

Petrography of Kimberlites from Leningrad and Lorik Pipe

The kimberlites from the Leningrad pipe belong to two types: tuffitic kimberlites and autholithic breccias. In the tuffitic kimberlites (Figure 3A), the debris are angular and their amount prevails on the deep-seated mantle material. In autholitic breccia (Figure 3A), the xenocrysts are dominating. Olivine with Mg#(=Mg/(Mg+FE)) 0.85-0.92) are dominating, pyroxenes, the Ca-perovskites, apatites, amphibolies, ilmenites, magnetites, biotites, phlogopites, serpentines and chlorites as well as carbonatites are common (supplementary file3.) In the Lorik pipe (Figure 3B) also compiled by autholitic breccia, the major mineralogy is similar but it contains also barites, zircons, zirconolite, Cr-rutiles similar to the kimberlites from Priazovie [34-36].

In leningrad kimberlites the Cr- diopsides are relatively rare but Cr-bearing amphiboles of various compositions are frequent.. They are found in xenoliths and xenocrysts and are abundant in the concentrates.

The rare diamonds in the Leningrad pipe [6,7,32]. Correspond to low temperatures 1075–1175°C according to the N content and δ13C‰$_0$= -4 which is heavier than for kimberlites in YKP and worldwide (δ13C‰$_0$ =-5.5) suggesting the growth from the fluid [9].

The Lorik and Svetlana pipes contain much less tuffitic material and amphiboles are not common among the xenocrysts.

Common typse of mantle xenolith in Leningrad pipe are garnet (Gar) (Figure C) and spinel (Sp) harzburgites (Figure 3D) though the spinel type prevails. with amphiboles (Amph) commonly associated with the clinopyroxenes (Cpx), Cr-spinels (Chr) ilmenityes (Ilm) and are often in the intergrowth with the phlogopites (Phl). inclusions of the apatites, Cr-rutiles, barites Sr - carbonates and various sulfides were detected by electron microscope (Figure 3E,F). The othopyroxene (Opx) and olivine (Ol) are mostly substituted. The sulfides like chalcopyrite, nickeline, keilite, millerite, pentlandite, pyrite, smythite, villamaninite occur in intergranular space. The deepest edinites and richterites were not found in thin sections and occur only in the concentrates.

Methods of Analyses

Electron microprobe (EPMA) analysis: These mineral grains were analyzed in the Analytic Center of IGM SM RAS in Camebax Micro and Jeol JXA8320 apparatus according to the published procedure [35,36]. Electron beam 1 micron; accelerating voltage -15 kV; beam current -15 nA; 15 seconds counting time. The relative standard deviation did not exceed 1.5%; the precision was close to 3-5% 2 sigma error. Altogether it was analyzed about 2100 grains (Gar-670, Cpx-142, Amph- 498; Ilm - 420; Chr -380) in addition the analyses of S. Babushkina made in IGDPM SB RAS using Jeol JSM-6480LV microprobe for Leningrad (1220), Svetlana (390) and Lorik pipes (235).
Electron microscope analysis: The detailed mineral compositions of ~ 420 grains in thin sections (370) and epoxy mounts (50) were studied using a MIRA 3 LMU scanning electron microscope with an attached INCA Energy 450 XMax 80 microanalysis energy-dispersive system (SEM-EDS) at the X-ray Laboratory of the Institute of Geology and Mineralogy, Siberian Branch, Russian Academy of Sciences [37,38].
Inductively coupled mass spectrometry with laser ablation (LA ICP MS): Mineral grains (77) of the kimberlite indicator minerals (KIM) from the concentrate of Leningrad pipe garnets (Gar) (31) and Cpx (18) Ol (2), Amph (69) were analyzed by laser ablation inductively coupled plasma mass spectrometry (LA-ICP-MS) in Nikolaev Institute of Inorganic Chemistry SB RAS using aniCAP Q mass spectrometer (Thermo Scientific) and an NWR 213 (New Wave Research), Nd YAG: UV 213 nm laser ablation system (analyst N.S.Medvedev). Detection limit ~10-7 and the standard deviation of the measurements for most isotopes was about 10-25% [32]. In total 54 isotopes of elements were analyzed. The NIST 612, 610 SRM were used as the standards. For the internal control 24Mg, 29Si, 39K, 47Ti, 55Mn, 52Cr and 44Ca isotopes were used to check agreement with EPMA analyses. The 44Ca, 29Si, 24Mg, isotopes were used for the normalization of the calculated values. Additionally, garnets and clinopyroxenes from samples 315-254, 315-167 and 315-73 analyzed in MRAC Belgium by solution ICP-MS [39] were used as internal standards. All data are presented in tables of the supplementary files (SF1-3).
40Ar/39Ar isotopic dating of minerals from xenoliths: Age samples of aillikites estimated by 40Ar/39Ar age using the method described in detail by Travin, et al. [40]. Quartz ampoules with samples were irradiated in the Cd-coated channel of a reactor (BBP-K type) at the Tomsk Polytechnic Institute. The gradient of the neutron flux did not exceed 0.5% of the sample size. Step-heating experiments were carried out in a quartz reactor with an external heater. The blank for 40Ar (10 min at 1200°C) was not higher than 5×10–10 cm3. Ar was purified using Ti and ZrAl SAES getters. The isotopic composition of Ar was measured on a Micromass Noble Gas 5400 mass spectrometer (analyst Yudin DS).

All analytic data are represented in the supplementary data file 5.

Results

Ar-Ar ages for Amphiboles and Phlogopite from Mantle Xenoliths

The results of the dating of the phlogopite grains and amphiboles occurred in the intergrouwth with the Phl are shown in Figure 4. The phlogopie from the spinel lherzolite 2665 Ma corresponding to the final stge of the craton formation. Similar age was determined for the Phl from Udachnaya [41]. The age of theintergrowth of the Amph-Phl from the sample Ol-151 is splitting. The high temperature part with the age 1368 Ma may be reffered to the the global activisation of the plume and accretion magmatism activity found in many World regions [42] including Siberia [43]. Yanger plateo ~ 380-400 Ma corresponds to Devonian plume magmatism. Small plateau ~210 Ma refer to Triassic plume stage.The sample Ol-112 give 370 Ma plateo – Devonian plume age. The yanger 160 Ma corresponds to the Jurassic stage of kimberlite volcanism [1-4].

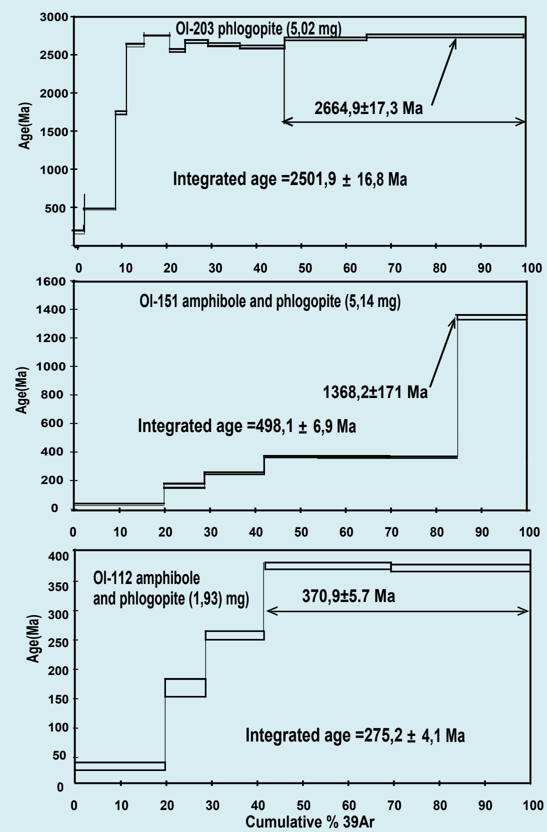

Figure 4: Results for the 40Ar/39Ar dating of amphiboles and phlogopite fomr mantle xenoliths from Leningra pipe Ol-203 reveal very and cient age 2.6.

Mineralogy

Garnets: Pyrope garnets were plotted on the CaO - Cr_2O_3 diagram (Figure 5A) covering the intervals from 0.2 to 12.5 wt.% Cr_2O_3. But there is one value at 18.8 wt.% Cr_2O_3 locating within the harzburgite field. The majority of the analyses locate within the lherzolite field according to Sobolev, et al. [44-47]. They are grouped into 8 clusters (Figure 5). Small number <30 of analyses are located within the dunitic filed Sobolev et al. [38].

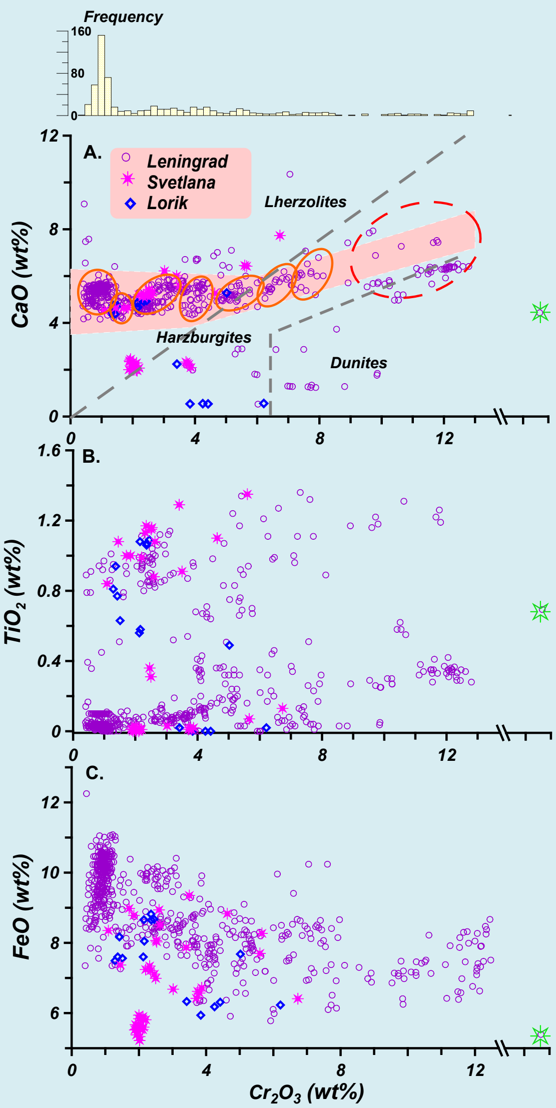

Figure 5: Variations of pyrope garnets compositions from Leningrad pipe in comparison with those from Svetlana pipe. 1. Pyropes from Leningrad pipe. 2. Pyropes from Svetlana pipe. The circles mark the clusters corresponding to the different layers in the mantle structure. The star marks the composition of the Cr- rich garnet (> 18% Cr2O3). Fields in CaO-Cr2O3 plot are according to N.V.

The huge number belongs to the low Cr varieties as is seen in the Cr_2O_3 histogram. They have the steep trend of the FeO rise together with CaO but have very low TiO_2 content (Figure 5B). Several clusters of the dunitic sub- Ca garnets were also detected starting from 2 wt.% Cr_2O_3. Garnets with Cr_2O_3 > 9% are plotting within the harzburgite field including the highest value 18 wt.% Cr_2O_3. Pyroxenitic garnets are rather scarce and occur mainly in the middle part of the diagram. The TiO_2 enrichment from 0.8 to 1.5 wt.% with Cr_2O_3 is found mainly in the low Cr part of the diagram. Comparing published diagrams of garnets and for Svetlana and Lorik pipe [7] those from Leningrad pipe are less abundant and diamond-bearing associations because the capturing interval is shifted to the low-pressure values.

The pyrope – almandine eclogitic garnets are widely distributed. They show the variations in Fe from 12 to 32 wt.% FeO and are separated into two intervals. According to the TiO_2 – Na_2O ratios they belong to the eclogitic non-diamondiferous assemblage.

Clinopyroxenes: The Cr -diopsides from the Leningrad pipe are formed the trend in FeO - TiO_2- Na_2O, Al_2O_3, Cr_2O_3 diagrams to 4 wt.%. In the MgO-Na_2O classification diagram. All Cpx belong to group A (Figure 6A). The Cr_2O_3 and Na_2O are rising to 4 wt. % at 2.5 FeO wt.% (Figure 6B-E) referring to metasomatic trend common abundant in Phl and Amph xenoliths [10,11]. We divided Cpx into 4 groups. The middle part of the diagram with the higher Ti, Cr, corresponds to H_2O metasomatism.

Amphiboles. For the classifications, we used the scheme based on the silica content [40] (Figure 7), the precise names may be found in the spreadsheets (SF1) [41]. The amphiboles from Leningrad pipe form nearly continous trend from Cr-bearing pargasitic hornblendes to pargasites, edinites, kataforites and later to Na-K and potassic richterites. The typical K richterites (Figure 7A,B) are changed to Fe- rich richterites. Trend cover practically all ranges of mantle amphiboles.

In addition, we subdivided the Fe- rich varieties that occurred among the high silica-rich and low silica varieties. The abundance of the Cr (Figure 7A) is rising in the middle part as in amphiboles from Daldyn -Alakit region [10,11] but TiO_2 in Leningrad amphiboles are lower (Figures 7C & 7J). The amphiboles from the Zarnitsa pipe also essentially differ from K- rich and sodic richterites from the Daldyn area [12-15]. The end members are characterized by the essential increase in Fe especially richteritic varieties (Figure 7D). Leningrad amphiboles are also essentially more sodic than those from Daldyn -Alakit fields. The electron microscope allowed us to determine the halogen content of the amphiboles from xenoliths and intergrowth. They all contain chlorine (0.1-0.3 wt.%) and no F at al.

Chromites: The chromites from the Leningrad pipe ond WUF kimberlites are forming several trend in variational to Cr_2O_3 - plots (Figure 8). The plot Cr_2O_3 - Al_2O_3 is lineal as usual but mainly for varieties with Cr_2O_3 40 wt.%. In the corner with high Cr_2O_3 values, there is continuous clouds at the joining of the ulvospinel magnesio-chromite and Fe-chromite trends in Cr_2O_3- Al_2O_3 -TiO_2, -FeO plots (Figures 8A-8C). In the Cr_2O_3 - FeO plot there are three separate trends, revealing different isomorphic substitutions and oxygen fugacity's regime. Most of the values are from the diamond stability field and essential part close to the field of diamond inclusions.

The Cr_2O_3-MnO plot shows the higher values for the Leningrad pipe compared to the Lorik and Svetlana pipe.

Ilmenites: The ilmenites from the Leningrad pipe give a long compositional trend on TiO_2 and MgO but there are many low-Mg values and an essential amount of compositions are plotting outsides from the typical kimberlitic and typical SCLM values [48,49]. The Cr rich varieties are typical for the high-temperature mantle metasomatites of protokimberlitic melts [10,11,49]. The two Al_2O_3 levels possibl mark magmatic impulses (Figure 9). The MnO is reaching in several varieties 12 wt.% and many grains have 2- 4 wt.% which is not common for the typical protokimberlitic systems.

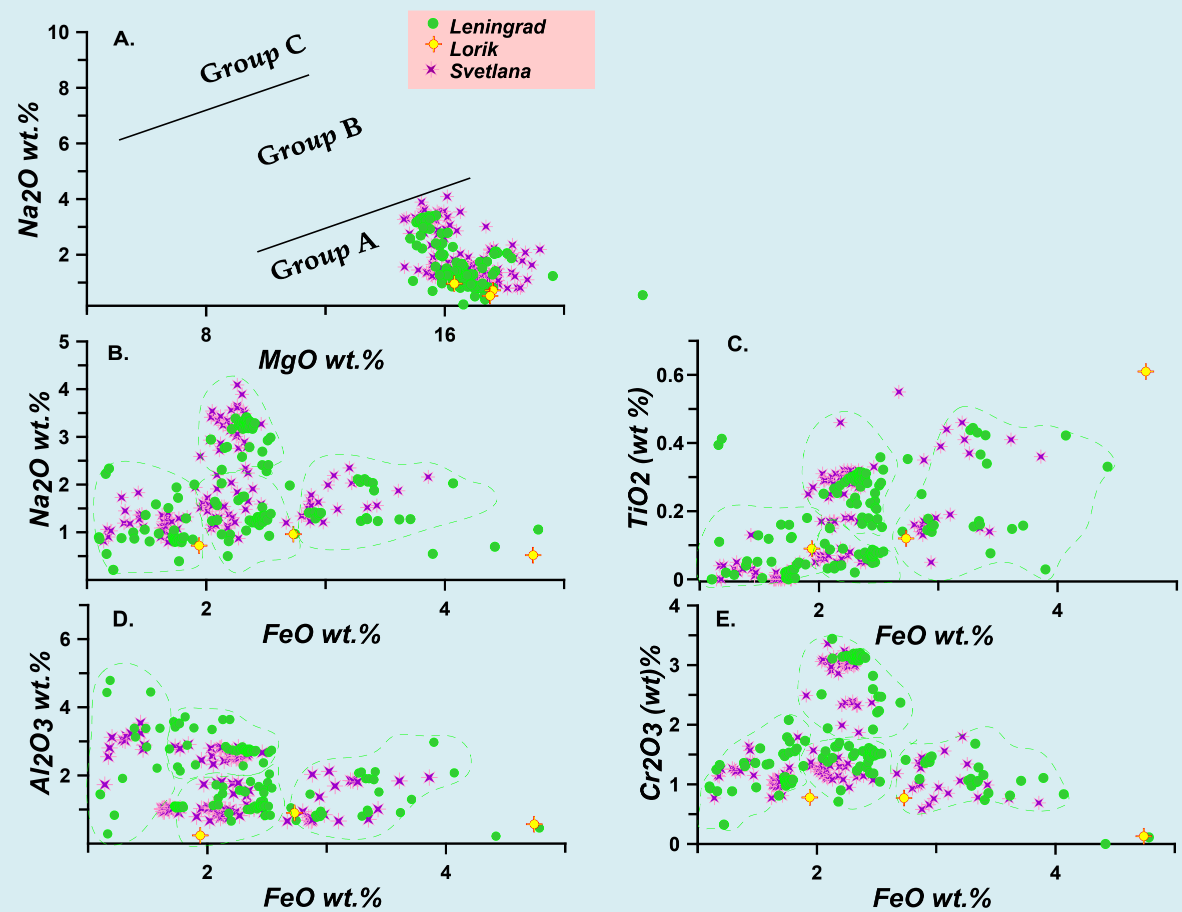

Figure 6: Variations of compositions of Cr-diopsides from Leningrad pipe in comparison with those from Svetlana pipe. 1. Cr-diopsides from Leningrad pipe. 2. Cr-diopsides from Svetlana pipe. Divisions according to Leake BE [45].

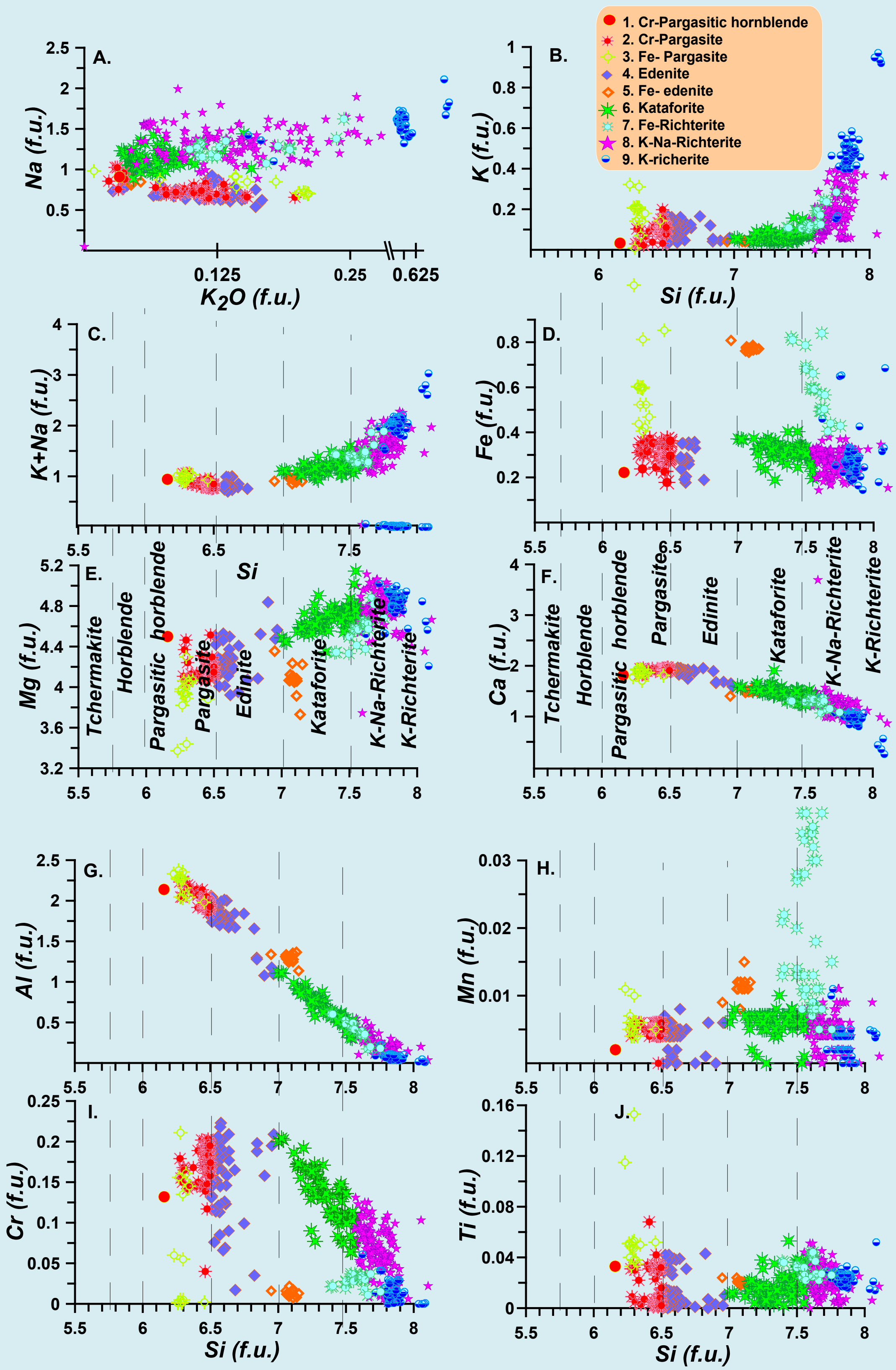

Figure 7: Variations of Cr-amphiboles from Leningrad pipe on the classification diagram [46,47].

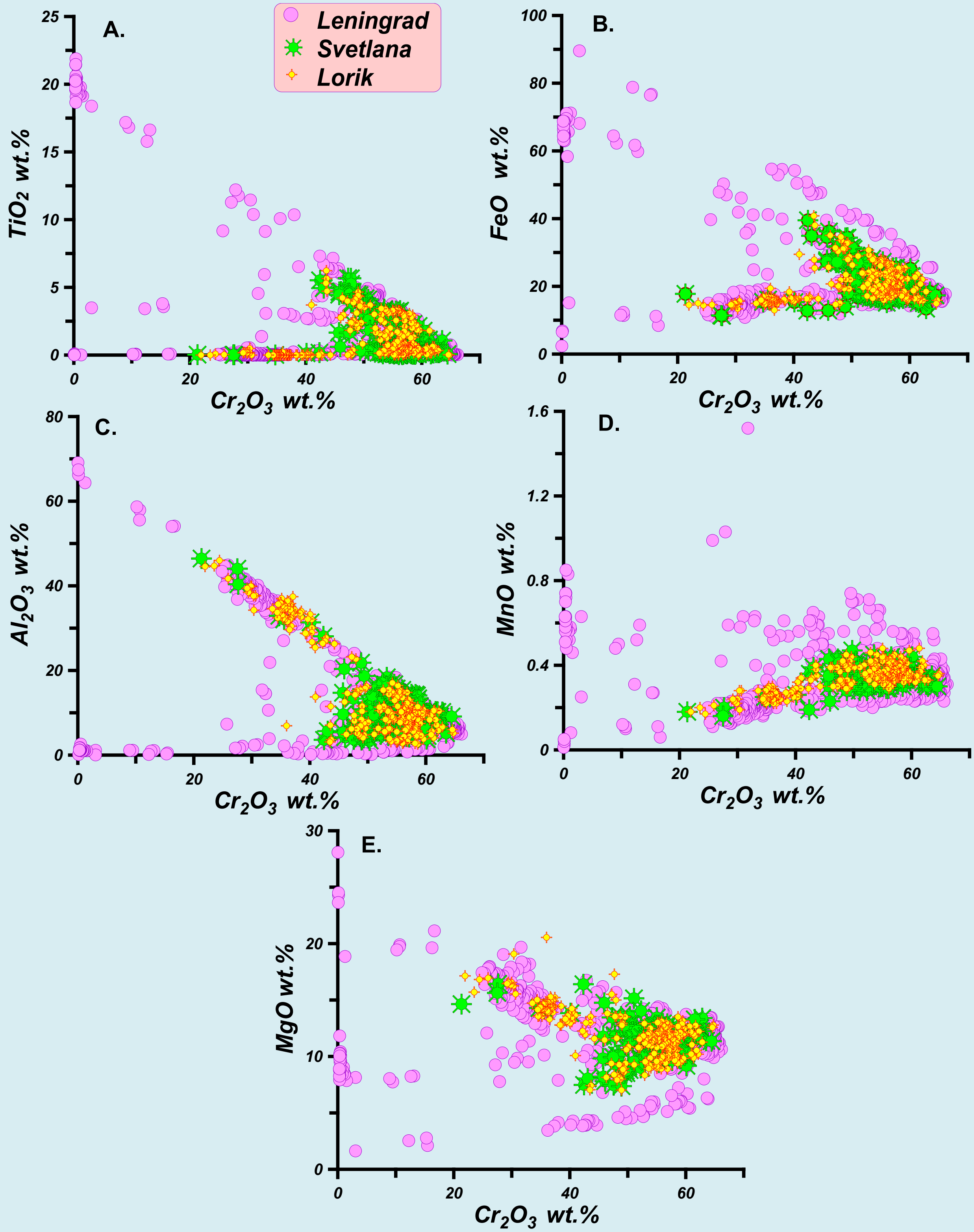

Figure 8: Variations of Cr-spinelides from Leningrad pipe in comparison with those from Lorik and Svetlana pipes.

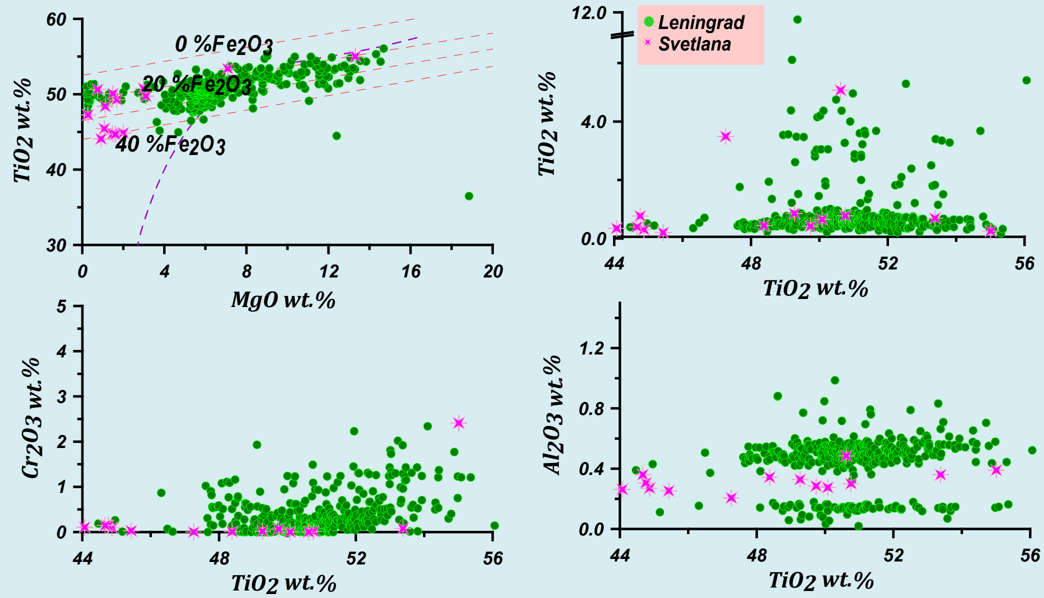

Figure 9: Variations of Cr picroilmenites from Leningrad pipe. Divisions to kimberlitic and non- kimberlitic types according to Wyatt, et al. [48,49].

Thermobarometry

Single grain thermobarometry: For the reconstructions based on the KIM minerals from the concentrate, we used the system of the published thermobarometers for the major peridotitic minerals: clinopyroxenes (Cpx), orthopyroxenes (Opx), garnets (Gar), chromites (Chr), ilmenites (Ilm) [50-52]. For the Cpx in the peridotitic system, jadeite – diopside barometer [37,44-46] is used. The corrected Jd- Cpx barometry is used also for the omphacites in the eclogitic system [50]. The modified Cr- garnet barometer [50,51] is used for pyrope garnets. The eclogite garnet barometer gives appropriate results for the Ca-, Na-bearing garnets using the dependence of Na in garnet from pressure with FeO varying from 12 to 30 wt.% [50]. For the Cr-spinels and chromites, we calibrated their dependence of Cr# (=Cr/Cr+Al) on pressure separately in garnet and spinel mantle facies [52]. The barometer is in combination with the spinel-olivine thermometer of Taylor, et al. [53] where the Fe#=Fe/(Fe+Mg) for the coexisting olivine (Fe#Ol) is calculated from Fe# for ilmenites (Fe#Ilm) and T°C by the empirical equations.

The oxygen fugacity: The oxygen fugacity of the Gudmundsson G and Wood B [54] in in the monomineral version was used to estimate the fO_2 for garnets. The fO_2 for ilmenite and chromite were calculated according to [53] in monomineral version. For the ortho- and clinopyroxenes the polynomial approximations [55] based in garnet estimates [54] were used.

All these thermobarometers are combined in the PT program Ter55 written in FORTRAN-70 [56].

Monomineral Amphibole Thermobarometry

The experimental high-pressure works give the stability of the Ca- amphiboles commonly to 3.0 3.5 GPa [21] and pargasitic to 4.0-4.5 GPa [22] while for the richterites the stability field was found to 8.5 GPa [23]. But a recent study shows that pargasites are stabile to 10 GPa [24].

Existing thermobarometers for Ca- amphiboles alow to work in low-pressures [18-22] varieties. The first author developed a new thermobarometric method [57] using the KD accounting Si-Al and K, Na-Ca re-distributions and the influence of other components and equations in analogy with the universe clinopyroxene barometer [50]. In this paper, this method was essentially improved. Usinf experiments to 8 GPa [22-24] and was checked using the material from the kimberlite xenoliths [10-17,29] for cross-correlations of PT estimates for different minerals.

As the thermometer, the method of Ravna K [58-64] based on the Fe-Mg (accounting Ca and other components) distribution between garnet and amphibole is used. It was transformed to the monomineral version. We added the corrections to the published version (Figure 10). The list of the used papers see in SF5.

The equations of the amphibole thermo barometer are given in the appendix.

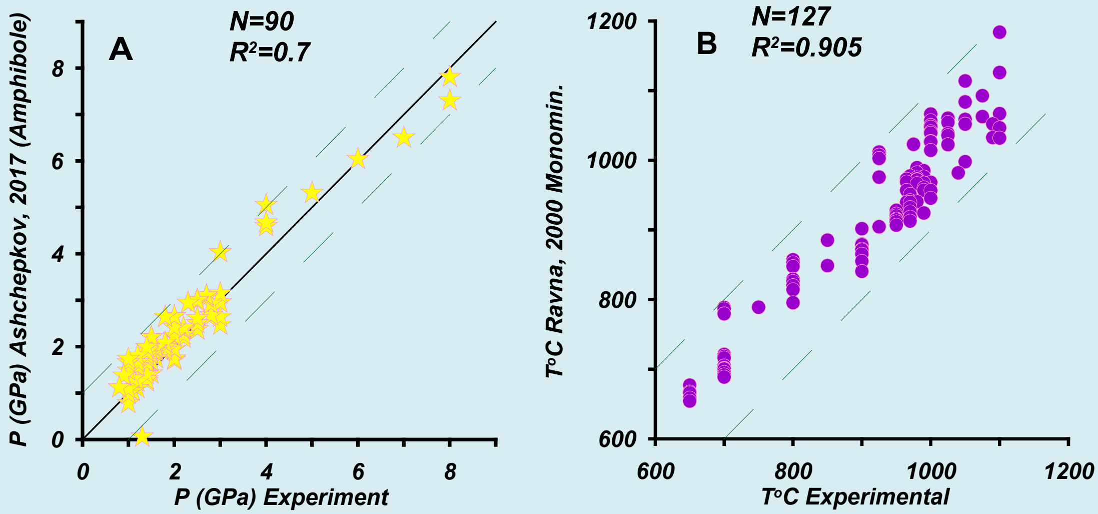

Figure 10: Correlations of the calculations with the experimental values or the amphibole thermobarometer.

Reconstruction of Mantle Sections Beneath the West Ukukit Kimberlite Field

The complex nature of the processes in the mantle lithosphere beneath the Leningrad pipe is visible in the PT diagram with the very rather complex geotherm branches (Figure 11).

The garnets are forming a wide PT field that is located in the lower part starting from 6 between 40 and 35 mw/m^2 conductive geotherm and in the upper part near 2.0 GPa, it is slightly above 45 mw/m^2 geotherm. From 6 GPa and deeper there is a wide scattered convective branch traced together by the Ilm and Gar PT estimates. The additional convective branch is traced by the garnets from 4 to 5.5 GPa just at the diamond – graphite transitions [65-69].

Amphiboles of different types trace practically all geotherm branches formed by Cpx and garnets. The low pressure are covering the 2.5-0.8 GPa interval and are divided into relatively high - Al-rich hornblendes and lower -Al - pargasites varieties. The edinites are tracing the middle part of the SCLMin pressure interval from 2.5 to 4.5 GPa. The kataforites and richterites are deeper and are found in 4.5-6 GPa interval. Their PT split to high-temperature (HT) and LT branches which close to those formed by Cpx's and pyrope's PT estimates. The K-Na richterites give high-temperature (LT) geotherm which is correspondent to those of pyrope diamond inclusions [70]. In addition, The Fe-enriched richterite varieties give the deviations to the high-temperature convective branch traced by ilmenites and HT garnets. The general feature of PT conditions for amphiboles is their division to HT and LT branches in all pressure intervals (Figure11). The general feature of PT conditions for amphiboles is their division to HT and LT branches in all pressure intervals. In the SCLM mantle beneath Leningrad pipe, West Ukukit field, Yakutia, the thermobarometry for garnets, Cpx, Chr, Amph allows us to identify seven horizons corresponding to paleo subduction slabs [71,72] (Figure 11). The oxidation state of the pyrope garnets is common and form the trend between 1-10%CO_3. The eclogitic and pyroxenitic Cr-low garnets are more oxidized and close to QMF buffer (Quartz-Magnetite= Fayalite) [68,69,71]. The chromites are the same in general but at 3-2 GPa they are anomalously reduced. The part of the clinopyroxenes is following to pyrope trend. But the those located within 6.5-4 GPa intervals are more oxidized and are plotting near the boundary Enstatite- Magnezite- Olivine- Garnet = Diamond (EMOG/D) [68,69] buffer to 0 QMF. The ilmenites reflecting the conditions of the picroilmenites shows FO2 values following EMOG/D buffer, in general, being more oxidized at the lithosphere base.

Two pipes from the SW part of the field also contains KIM used for the thermobarometric reconstructions. Both of them contains mainly chromates. The chromites from the Lorik and Svetlana pipes show the low-temperature conditions at the lithosphere base at 6 GPa which is followed by the advective trend to 3 GPa (Figure 12). The pyrope garnets are represented mainly by the sub-calsic varieties tracing low-temperature geotherm. In the upper part, the geotherm is composed of the PT estimates for the wehrlitic garnets and Ti-rich Cr-spinels. Pyrope garnets mostly give the 3-4 GPa interval and are sharply divided into sub-calsic and pyroxenitic varieties. The latter sow the conditions up to 7.5 GPa referring to 40 mw/m^2. The clinopyroxenes trace all parts of the geotherm for garnets and Cr-spinels. They also create the relatively Fe-rich hot branch at 6.0 GPa commonly associated with deformed peridotites.

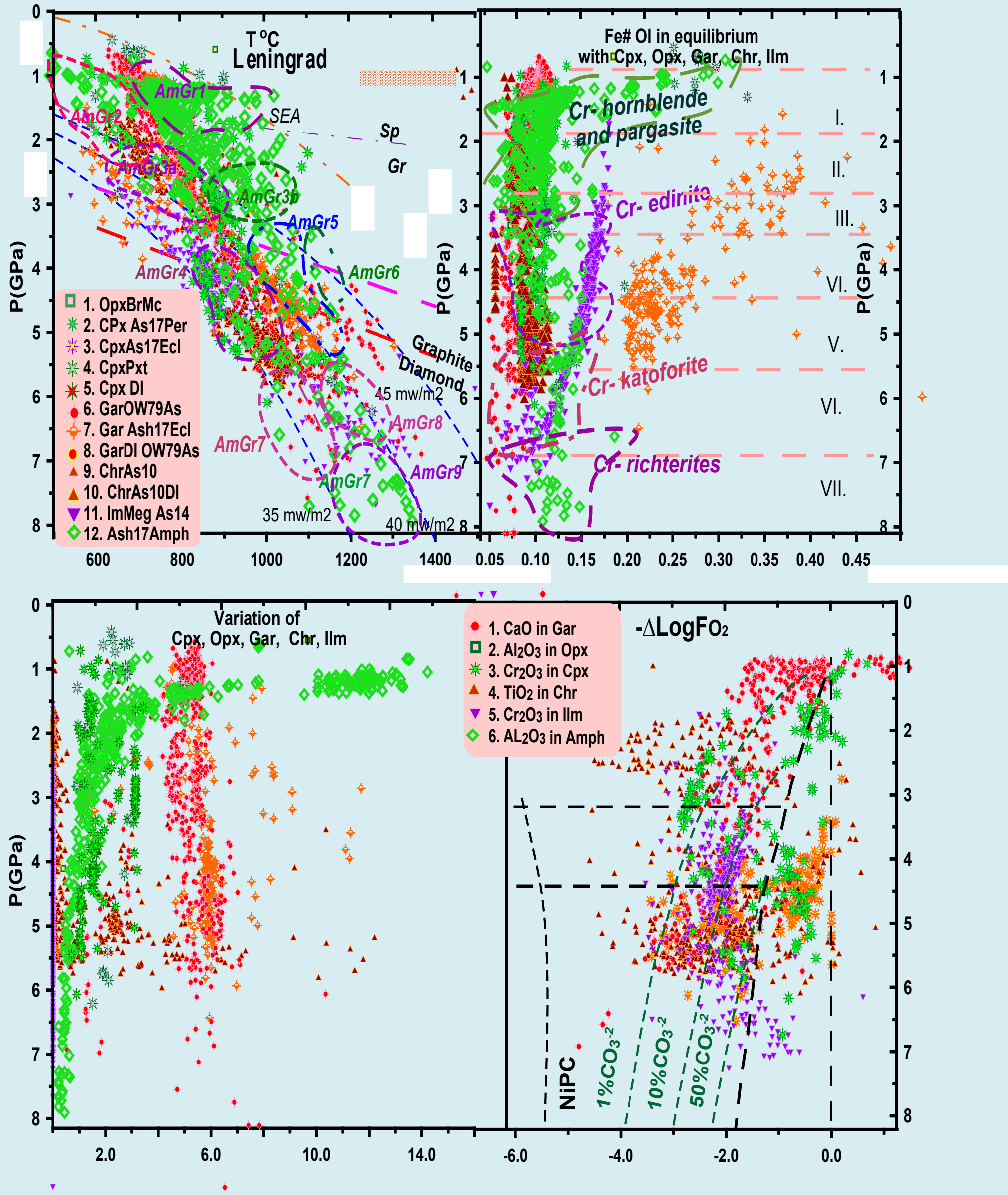

Figure 11: PTXfO2 diagram for the minerals xenocrysts from Leningrad pipe. Signs: 1. Opx: ToC [59]-P(GPa)[60]. 2. Cpx: ToC - [61] - P(GPa) – [50] (for Cr -diopsides); 3. The same for pyroxenites and Fe- Cr -diopsides. 4. The same for eclogites and pyroxenites; garnet: 5. ToC [62] -P(GPa) [50]. 6. [58]- [44] for eclogites; chromite: 7. ToC [63] -P(GPa) [52]; 8. Ilmenite megacrysts: 7. ToC [53]- P(GPa)[52]; Amphibole: 9. ToC –P[58] –P (GPa) [51] corrected. The horizontal dashed line at 3.5 and 4.5 GPa corresponds to the Graphite-Diamond boundary [65,66] at 35 and 40 mWm-2 respectively. Conductive geotherms [67] The field for P-FO2 diagrams and lines of CO3- concentration in melts are from [68,69].

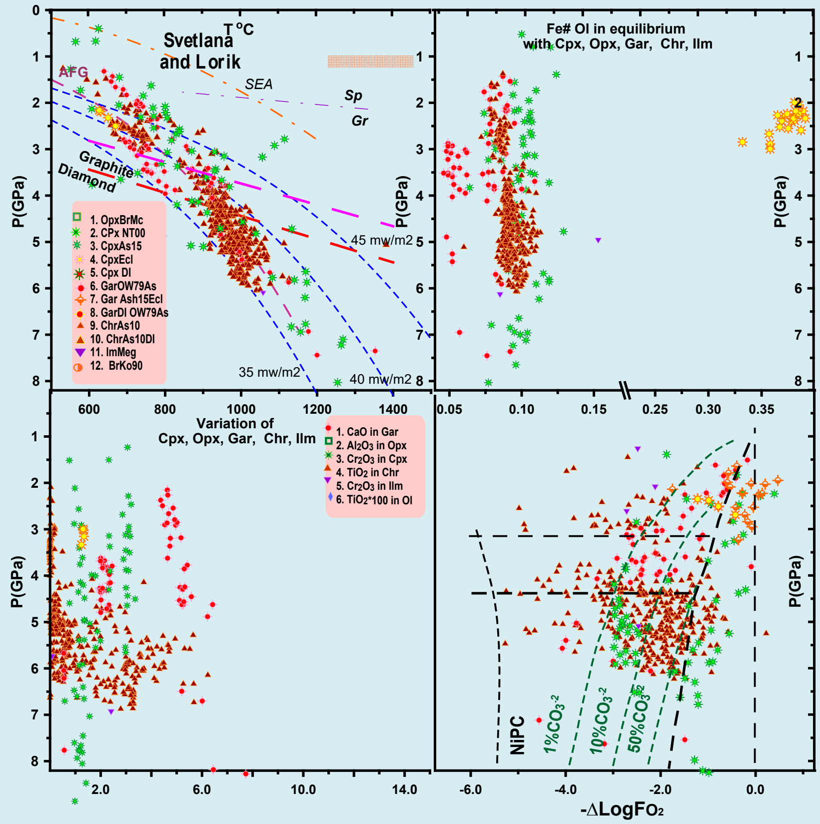

Figure 12: PTXfO2 diagram for the minerals xenocrysts: a) Lorik pipe; b) Svetlana pipe. Symbols are the same as in Figure 11.

Geochemistry of the minerals

Garnets: We divided garnets into 7 groups according to trace element patterns. The group with the highest REE level at 100/CI (Chondrite Iruma) [73] refer to the crust granulites and they show deep minimums in high field strengthen elements (HFSE). Analyzed peridotitic garnets from the Leningrad pipe of the prevailing lherzolitic type reveal mostly regular semi-round (concave upward) rare earth elements (REE) patterns with the low LREE level. Common lherzolites (GLh) in the spider diagram for trace elements (SDTR) reveal the evident elevations in Zr-Hf typical for the metasomatic phlogopite bearing mantle and rather high Ta, Nb, U and Th. The trace element (TRE) spider diagrams show mot very low minima in Sr, Pb and deep in Ba and low large ion lithophile elements (LILE) except for Rb. Harzburgitic garnets (GrHz) display small minima in MHREE and essentially lower all incompatible elements from the left part. The depleted harzburgites GrHrD show also lower LREE part and all incompatible elements. Garnets from dunites (GrDun) show and moderately low levels of incompatible elements and HFSE and some of them show even elevated levels of LILE. There are two types of pyroxenitic garnets. The 1st one GrPxt1 reveal the hump in the REE pattern and the SDTR show the high incompatible element level including HFSE with the peak at U. the second GrPxt2 display the flattened REE and slightly elevated LREE and LILE while HFSE are slightly lowered (Figure 13).

Clinopyroxenes: The clinopyroxenes were divided into 5 groups. The samples from Gr1Cpx show REE level at 300/C1 or more in La and inclined La/Yb_n~10 patterns. In SDTR the HFSE reveal minimums in and rather low LILE but Th,U are slightly elevated. The Cpx from the Gr2Cpx are lower in La level but are more inclined La/Yb_n ~12- 15. The HFSE are varying and mostly low similar to those in intergrowths with the ilmenites [14]. The Gr3Cpx (pyroxenitic) display higher REE inclination and nearly straight line REE patterns. The SDTR is more smooth and the left part of the diagram (incompatible) is very low. The REE patterns from with lower REE with La_n ~15 concentrations have minima in Ta, Nb and more flat Zr -Hf. The samples from the Gr5Cpx have different REE – one (a) displays very high LREE >100 and La/Yb ratio the second nearly flat pattern at ~10 La_n level typical for spinel facie. But they have very huge U-Th peaks but like those for the carbonates. They have minima in Hf, Pb, Nb and LILE.

One Opx show lowered concave downward inclined REE pattern with La_n at 20. The SDTR display deep minima in Zr, Hf, Nb but elevated Th, U, Sr. And one olivine display also inclined concave pattern with the minima from Dy to Tm. The right part of the SDTR is lightly inclined but relatively smooth with the minima at Ta but peaks in Pb.

Olivine and Orthopyroxene

Amphiboles: The low-pressure Cr – pargasitic hornblendes (AmGr1) show highly inclined and deeply concave downward REE patterns. All of them have the peaks in Eu reveal rather high LREE level - La_n~100 CI and they have essential depressions in HMREE part with the minima near Ho-Dy REE patterns. The SDTR for most of them shows strong peaks in Ba, U and smaller ones in Ba. They reveal HFSE minima except for Y. The more HT varieties (AmGr2a) show similar patterns but much lower in REE and less inclined pattern with the LREE at 50-10/CI and they reveal the minima in Nd and Ta and highly variable f oor maximum in Zr Hf. The amphiboles from Gr2b show a much lower LREE level (La_n ~10/CI).

The amphiboles (mainly edenites) from AmGr3 are subdivided into 2 subgroups. Groups 3a and 3b have a similar inclination of REE patterns with $(Gd/Yb)_n$ ~5 -7 and slightly bell-like from La to Sm pattern. The MHREE are slightly concave downward from Yb to Ho. The amphiboles of AmGr3a with the higher REE level and La_n ~150 to 100 reveals the evident Eu minima. The samples from AmGr3B have no Eu anomalies. The TRE spider-diagram for AmGr3a show the minima in Zr-Hf and contrast Nb peaks and minima. Both two groups have moderately depleted LILE group with local Ba and higher U peaks. The AmGr3b have elevated Ta, Nb and slightly elevated Zr, Hf, Y very low Th.

The kataforites AmGr4 reveal similar REE patterns without no Eu anomalies.with the inclined from Nd to Yb part and more flattened from La to Nb part and The level of La_n ~100- 40 or higher. The spider diagrams have gently decreased from the Nd to Yb part with the small fluctuation in Hf and Sr The definite feature is a strong Nb peak and They have Th trough rather low U and elevated LILE. The REE patterns from AmGr5 are show bell-like spreading in LREE part and the same inclined branch from Sm to Yb as the previous. An opposite they reveal very high U and deep Nb trough but high Ta.

The samle Am.Gr6 are similar as previouse but hafe lowes REE they show roughs in Th, U.

The high-pressure amphiboles K-Na richterites typically reveal higher inclinations compared to all previous groups $(Gd/Yb)_n$ ~ 20-30 with the minima in HMREE near Er–Tm.

The amphiboles from AmGr7 corresponding to the low-temperature geotherm reveal nearly straight-line REE patterns with the very high level of LREE (La_n~1000/ CI) with the Eu minima and flattened HREE part for samples from AmGr7b. One spectrum of AmGr7b for the Na- richterite shows a less inclined REE patterns and small depression from La to Eu.

The samples from the Gr8Am reveal lower REE highly inclined REE (La_n~100-60/ CI) and $(Sm/Yb)_n$~ 70-50 display with the more flattened right and left parts. They have strong U, Ta, Sr peaks and elevated Rb, Hf, Zr, Y and minimums in Nb.

The more HT group AmGr9 reveal less enriched in REE and nearly conform patterns. They display the same peaks in Ba, U (for most) Ta, Sr, Zr, Hf and small in Y and negative in Th. One sample shows negative Ta and positive Th anomalies.

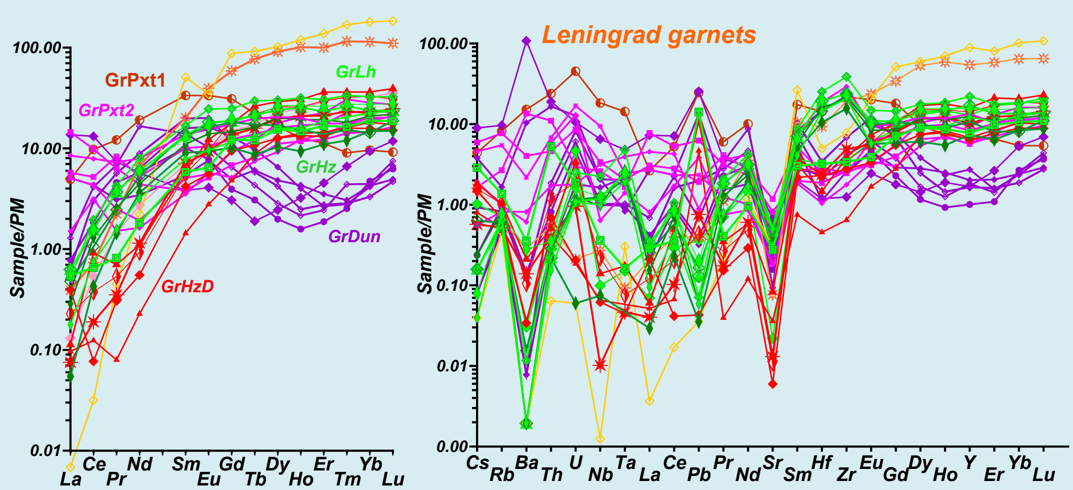

Figure 13: REE patterns and TRE spider diagrams for the pyrope garnets from Leningrad pipe. Normalization REE to [73] and TRE spider diagrams to [74].

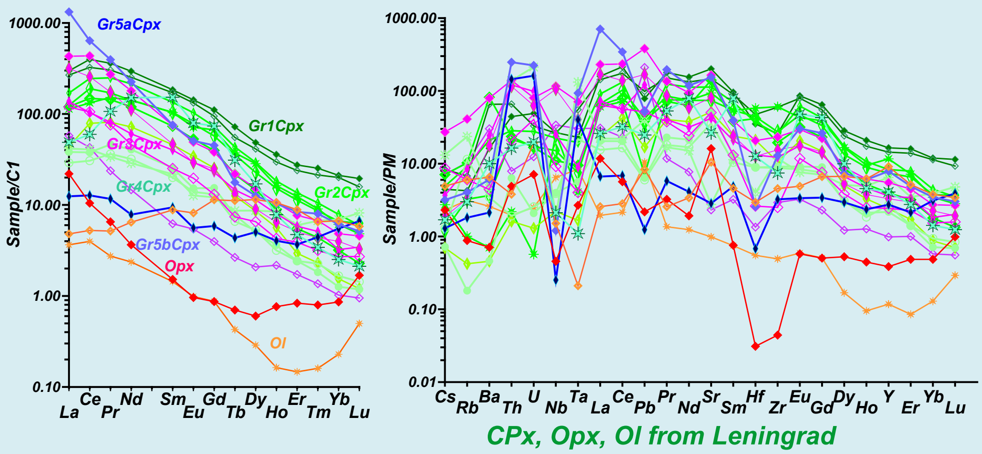

Figure 14: REE patterns and TRE spider diagrams for the clinopyroxenes, orthopyroxenes and olivine from Leningrad pipe. Normalization is the same as in Figure 13.

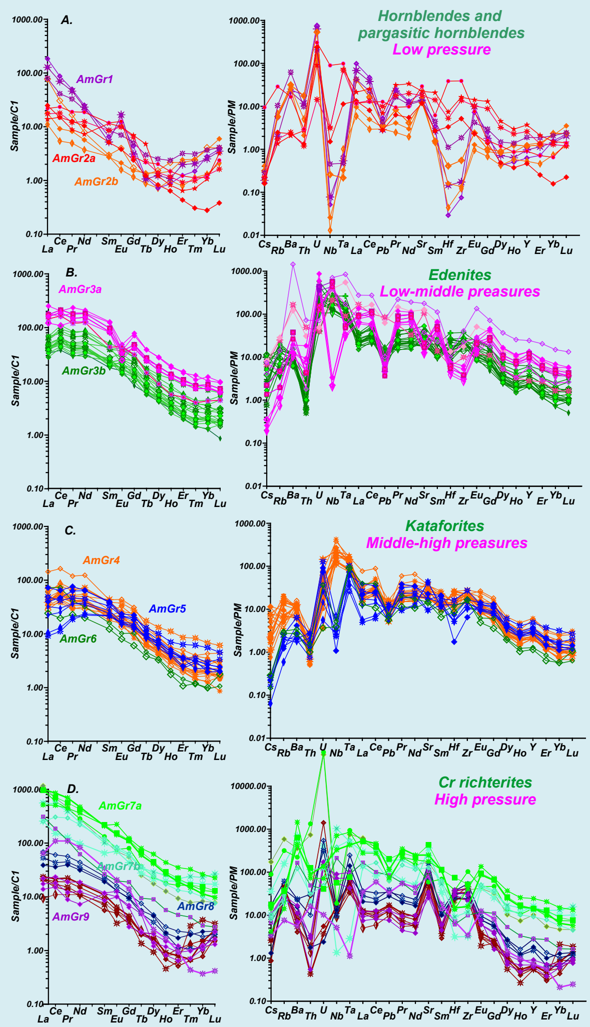

Figure 15: REE patterns and TRE spider diagrams for patterns for amphiboles from Leningrad pipe: a) low-pressure hornblendes and other Ca- amphiboles; b) low-middle-pressure pargasites; c)middle- high – ressure pargasites edinites; d) high-pressure Cr- richterites. Normalization is the same as in Figure 13.

Discussion

The Mineralogy as the Factor of the Diamond Grade and Geodynamic Conditions

The mineralogy of the Leningrad pipe, in general, is similar to pipes of the Devonian kimberlites from YKP [75,76] showing the long range of the Cr_2O_3-CaO in the lherzolitic field and extending to 18.2% Cr_2O_3 belonging to the harzburgitic field which is one of the highest in the YKP. It suggests the very deep source of this pipe like those from the Mir [67], Nakyn [77] or Zarnitsa [13]. Unfortunately, like some other large pipes including the Zarnitsa, the prevailing breccias capture mainly the upper part of the mantle section without diamonds. The pipe has the polyphased structure, which is visible not only from the observations of the kimberlite relationships in the pipe but also supported by the complex chromite and ilmenite trends in the variation diagrams. The majority of the chromites are rather high chromium that also expands the perspectives of the diamond grade. A rather high amount of the almandine-pyrope garnets refer to the eclogites and HP varieties according to the thermobarometry may be diamondiferous. It suggets that similar rocks may be sourcews of placers which contain beautiful diamonds [78-80].

There are many signs that the mantle in the northern YKP is more hydrated is higher than in central YKP region.

Comparisons with the Amphiboles Worldwide

The most interesting feature of the Leningrad pips – the high variations of the Cr-bearing amphiboles, which is the highest in the World among the kimberlitic pipes and any other mantle objects. Commonly amphiboles occur in the highly metasomatized mantle peridotites. The richterites were found in the MARID xenoliths in several pipes from the Kaapvaal craton [29,81-83]. The pargasitic types were described in the peridotite mantle xenoliths from Kimberly pipe [84] and in the xenoliths from Gibeon Kimberlite Province, southern Namibia [85,86]. They were found in the eclogites of Orapa, Roberts Victor [81] and other kimberlite pipes of South Africa [87]. Ca- amphiboles occue in peridotite of many orogenic massifs such as Lherz [25], etc. They are detected in the mantle xenoliths from the alkali basalts in Transbaikal in Bartoy volcanoes [88], in the European Cenozoic basalts including Massif Central [89], Rhon Graben [90] and Pannonian [28], in Victoria Land, Australia [91,92] in Nushan, China [93] and many mantle arc basalt localities [94] other locations of mantle xenoliths.

The breakdown of the amphiboles in the mantle in the island arc environment is the source of the H_2O during the formations of the granites above the deep subduction zones [95]. The amphibole metasomatism put an essential role in the distribution of the LILE and HFSE components in the mantle [90] due to the high partition coefficients of this mineral [96-100].

Recent researches show that pargasites are stable to 20.5 GPa [24]. The PT stability field is consistent with the conditions of both hot and cold subduction. The richterites are stable to 8 .5 GPa and more [23,96].

The presence of the crustal signatures in the geochemical features of the amphibole suggest the strong influence of the subduction material to very high-pressure conditions of the SCLM [100-102]. The abundance of the amphibole is caused by the continental margin environment of the W.Ukukit mantle in ancient times.

Thermobarometry and Mantle Layering, the Geothermal Conditions of the SCLM Beneath West Ukukit Field

The layering of the mantle column is mainly shown by the distribution and variations of the pyrope garnets in the SCLM. In the P-Fe #, diagrams there are several small arrays of the growth of the Fe with the decreasing pressure which probably refer to the primary layering coursed by the coupling of the paleo subduction slabs in the Archean time [103]. It is visible in the middle part from 3 to 4.5 GPa. The lithosphere base is probably found at the common position at 6 GPa. The hot garnet geotherm is found from 7.5 to 5.5 GPa marked by ilmenite trend produced by interaction with the protokimberlite system. Heating is found in the middle part where there is a hot branch formed by pyropes along the diamond graphite boundary. In the upper part of SCLM, the heating is pronounced from 3 GPa to Moho. However, several clots of rather low-temperature garnets are found at 7 GPa. The eclogitic garnet are forming two branches in the PT and P-Fe# plots. The Fe# growth during the pressure decrease was probably created during the rise of the melts, which were produced during submerging of the subduction layers to the depth [104,105]. It is proved that even peridotites paleosubducted layers were segnificantly re-melted [106] and eclogites should be nearly completely melted forming ascending magmatic bodies. On the PT diagram, eclogites are mainly forming the branch near 40 mw/m^2 in the lower and middle part of the mantle column and they reveal low-temperature conditions in the upper SCLM part starting from 4 GPa. Branching for the Cpx geotherm from LT 35 mw/m2 branch to HT convective branches (advective) from 6 to 4 GPa probably reflect influence of the protokimberlite melts and fertilization processes [107,108]. The most Mg-rich chromite compositions also are distributed in the middle part of the mantle section from 3 to 5 GPa. While in the lower and upper parts of the SCLM, they became more

Fe rich due to interaction with the protokimberlites. in the lower and middle part and probably with basaltic melts in the upper part of the SCLM The same feature is found for the compositions of the amphiboles which are forming the hot and Fe rich branches in the base of the lithosphere and the upper part starting from 3 GPa.

The ilmenite trends and distribution in the mantle column is complicated. The lower part from 7.5 to 6 GPa is rather high-temperature and Mg-rich and corresponds in the PT conditions to the dunite harzburgite garnets. Probably these are the high-temperature metasomatites at the lithosphere base, which are found in most kimberlite pipes. The deviations to the high Mg-Ilm compositions refer to the metasomatites. However, the major trend is the typical trend of the protokimberlite melt fractionation.

The he amphiboles provide the most complex PT conditions. They are sharply divided into three pressure groups. The lower part is correspondent to the 3 clusters. The sodic richterites with the Eu anomalies gives the lowest temperature branches to 35 mw/m^2 starts from 6.5 GPa and continuing to 4 GPa slightly heating. The possible model is reactions with rising of the hydrous subduction-related fluid rich melts through the mantle column. The hottest branch is correspondent to the K –richterites and edinites at the lithosphere, which are Fe- Ti, enriched due to reactions with group II kimberlite and heated to the 45 mw/m^2 geotherm. There are all the intermediate temperature variations. Next hot clot the amphiboles is at 5 - 5.5 GP and this cluster nearly coincides with the hot garnet branch for the pyropes. The next heated branch is near the diamond-graphite boundary. The heated branches are most pronounced between 3-1 GPa. In addition, the heating for amphiboles is from 45 to 90 mw/m2 geotherm in the upper part for both Cpx and Amph that corresponds to typical "basaltic" or SEA geotherm [109]. The behaviour of the Al in amphiboles on the P –Variation diagram (for amphiboles Al_2O_3) shows the changes from the LAB level to 3.5 GPa where the Al_2O_3 begin essentially grow up. Starting from 2.2, GPa the Al in amphiboles drastically splits from enriched in al compositions to typical hornblendic with the 10-14 wt.% Al_2O_3.

Using the Cpx, Gar, Chr, Ilm and Amph composition we determined 7 levels in the mantle column beneath the Leningrad pipe.

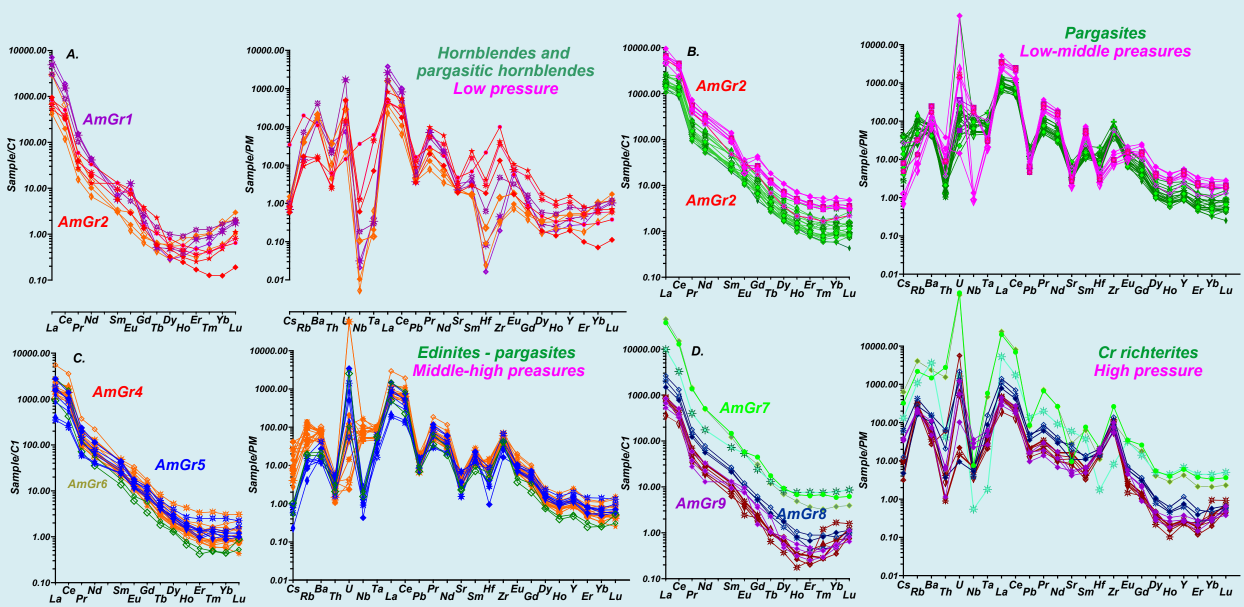

Figure 16: REE patterns and TRE spider diagrams patterns for melts in equilibrium with the amphiboles from the Leningrad pipe. A partition coefficient [97-111] Normalization is the same as in Figure 11.

Geochemistry of Minerals from Mantle Peridotites, Metasomatites and Vein Systems and Relations to Geodynamics

Garnets are splitting by the REE and TRE spectrums to typical lherzolites with the Zr- Hf peaks which mark H_2O metasomatism [75] and tharzburgitic groups with the different LREE content and probably melting degrees of host rocks. It is clear that dunitic and harzburgitic garnets with relatively low HFSE should be related to the ancient subduction-related processes which commonly reveal elevated Ba, U, Sr, Pb [110] but troughs in the HFSE.. Pyroxenitic garnets type 1-2 with the elevated or high levels incompatible elements but minima in Zr, Hf with the high levels in all incompatible elements probably have the hybrid nature of mixed subduction relayed processes. Garnets from the low crust probably refer to the cumulates from the plume basalts.

The clinopyroxenes reveal quite variable tendencies. One Cpx from Sp lherzolites demonstrate high Th-U peaks typical of carbonatitic melts [112] but the other with. The Cpx from garnet facies also reveals controversial tendencies. Two of them have elevated Rb and Sr, elevated Th but low U what probably means the influence of potassium bearing fluids. The trough in Zr and Hf combines with the strange Sr peak for olivine. These features are suggesting the influence of the evolved carbonatite melts Gr1, Gr5. The typical the clinopyroxenes with the high REE level and Th, U, Sr Gr1Cpx, Gr3 Cpx, Gr5 Cpx probably are related to the alkali-carbonatitic melt. Gr4- should relate to early-stage protokimberlitic melts and Gr4Cpx have mixed signatures. The inclination is commonly regulated by the Cpx/Gar ratios in the source which is higher for the pyroxenites,

Most of the low-pressure hornblendic amphiboles show concave REE patterns have the concave downward patterns which mean the fluid type crystallization as it is found for the boninites and anomalies of Eu suggesting the participation of Pl bearing crust material in the source of fluids. They could be created from the amphibolization for the pre-existing eclogites or directly due to the substitution of the clinopyroxenes [113]. The low- middle-pressure amphiboles show rather high La/Yb_n ratios which suggest the crystallization in presence of garnets or/ and participation of the LREE rich fluids in the origin of the parental melts. High Ba and elevated U and essentially high Na/K ratios support the presence of Na- subduction-related fluids [109] as well as the very deep HFSE anomalies with the varying Ta- Nb which is typical for the rutiles having different partition coefficients for the Nb and Ta [110]. The edinites and pargasites from the middle-pressure interval reveal the serious difference in the geochemistry. The edinites from the low-temperature branch have minima in Eu, which suggest the higher oxidation stage they have higher Rb, Ba T and display minima in Zr Hf and Nb but elevated Ta. The pargasites demonstrate the lower REE and TRE values and practically no Eu and HFSE anomalies and even peak in Ta and as well lower Ba, Th, U than pargasites and high Sr and Pb. This probably meant the participation of the rather high temperature melts in their origin because the higher the temperature the low are the REE and as well (La/Yb)n ratios The fan-like spreading REE part of the patterns suggest the participation of the partial melts from the peridotite source with the different Ga/Cpx rations in the source [74]. The most high-pressure richterites are very different. Those with high REE and inclination (La/Yb)n, LILE and all other incompatible components and minimum in Ta [101] suggest low degree melting and high Ga/Cpx ratio in the substrate [74].

The compositions of the melts reconstructed with the KD for the amphiboles [97-99] reveal very high LREE patterns and concave in the MREE part (Figure 16). The levels of the HFSE are mostly low but there are some varieties rather high in Zr which is probably evidence about the participation of the H_2O rich melts/fluids in their generation. They are not close to boninites but somewhat similar [113,114]. Most probably such amphiboles generation maters were fluids.

The halogens in the amphiboles of all types are represented only by chlorine which supported the idea of the influence of the subducted related fluids [113-117]. Commonly the fluorine is more compatible in Ca- amphiboles than chlorine [115]. The abundance of sulfides, apatites, barite also support the idea abot the subductionrelated metasomatism.

Model of the mantle evolution of the SCLM beneath the Ukukit field and the role of the subduction.

The SCLM beneath Ukukit have rater contrast layering typical of Siberian Craton [66] and the formation of the mantle beneath the Ukukit field (Figures 11-12) is not different from the central parts of the craton. The model suggests the hot subduction at the presence of superplume which caused the floating of essentially melted peridotite – eclogite slab and joining it to craton keel from beneath [72,75,103]. The alternative model suggests the stacked subducted slabs [75].

Presence of the Phl with the 2.6 Ga referring to the most andvient mertasomatic H_2O bearing metasomatic processes recorde in the mantle xenoliths in the World proves the common model of the appearance of water in the mantle at the last stages of the continents grows, The other two peaks 400 -380 Ma and 160 Ma bothe may be referred to the plume Kimberlite magmatis anmd even to the protokimberlite stage (latest one).

The essential difference is the broad development of amphiboles, which means the later very vast interaction with the subducted related melts, which were enriched in the LILE and sometimes U, Th, HFSE (Figure 15) due to participation of the continental material in the subducted material. It is difficult to imagine the abundance of primary amphiboles in essentially heated Early Archean mantle. The contrasting behaviour of Ta and Nb is regulated by the rutile partition coefficients likely for primary eclogites. Though it could occur because they were found in the Archean mantle eclogites [110]. And it was suggested they were the source of the archean crust [118]. But mostly metasomatized eclogites are related to later events [119,120]. They were subjected to the melting and are mostly magmatic bodies rising through the lowerpart of mantle columns [121].

The hydrated mantle may occur in the continental arc environment where H_2O together with Cl, S, P could provide essentially influence the primary mantle peridotites and eclogites [118]. The subduction-related fluids passed through the all mantle column and caused vast perturbations. Subduction and Na and K (siliceous) types of fluids percolated through the mantle with abundant eclogites causing amphibolization through the whole mantle column. The plumes produced hybridism and more smooth patterns. The presence of the different types of amphibole suggests that it was subjected to multistage fluid interaction of both Na and essentially type which suggests the changes of the type of subduction-related processes. The HT amphiboles appeared as a result of the interaction of the hydrated mantle with the plumes in several stages. The huge compositional variation amphiboles from the Leningrad pipe nearly cover all types of mantle amphiboles [13]. The pressure interval for the amphiboles nearly covers all types of mantle amphiboles determined for the new version of the amphibole thermobarometry [51] (see appendix)support the experimental data [120-134] and presence of amphiboles in diamond inclusions [135] and deepest metasomatites [128,136,137]. And as we can see from the Leningrad kimberlite xenocrysts they form continuous series in the thick lithoapheric mantle beneath Sibeian [138] and possibly other cratons. Earlier ie was suggested that in the northern part of Siberian craton mantle lithosphere si not thick [139] and even delaminated, but the examples from Leningrad and all studied pipes prove that it was very thick even in Jurassic and Triassic impulses of kimberlite magmatism, which suppose that it possible to find high in diamond grade pipes in the Northern part of Siberian craton.

Conclusion

1. Leningrad pipe contains a huge number (>500 EPMA analyses) of various amphiboles (9 groups according to geochemistry) from Cr – pargasitic hornblendes through Cr- pargasites, edinites, kataforites to Cr - richterites referring to the different PT conditions from lithosphere base to the Moho. This suggests high H_2O activity in the mantle column and the relatively low-temperature nature of mantle metasomatites.
2. The geochemistry reveals the vast variations of the TRE and REE spectra. The low-pressure Cr – pargasites have the signs of fluid interaction with the melst/fluids with the concave REE patterns and peaks of Ba, HFSE minima reflecting high oxygen fugacity. The Eu anomalies suggests the crust material participation. The HFSE enrichment possibly suggests the interactions with the evolved essentially carbonatitic plume mostly protokimberlite melts.
3. The chemistry of pyropes (18 wt. % Cr_2O_3) suggests their deep probably asthenospheric origin.
4. Complex geotherms and trends of amphiboles, chromites and ilmenites and variable geochemistry of minerals suggests the multistage interaction with the subduction-related and later plume melts.

Supplementary Materials

The following are available online at

Author Contributions

Conceptualization, I.A.; methodology I.A., S.B., O.O. and N.M.; software, I.A.; validation, I.A., S.B., O.O, N.M.; formal analysis, I.A., S.B.,N.K and N.M; investigation, I.A., S.B., O.O, N.M, N.K; resources, I.A.; data curation, I.A., S.B., O.O. and N.M.; writing—original draft preparation, I.A..; writing—review and editing, I.A.; visualization, I.A.; supervision, I.A., O.O.,; project administration, I.A.; funding acquisition, I.A. All authors have read and agreed to the published version of the manuscript.

Funding

This research was funded by Supported by RFBR grants 19-05-00788,. Work was done on state assignment of IGM SB RAS, governmental assignment in terms of Project IX.129.1.4. The research was supported by the Ministry of Science and Higher Education of the Russian Federation, N 121031700315-2.

Data Availability Statement

Ithe data fr Siberian craton and many of published paper may be found in Research Gate https://www.researchgate.net/profile/Igor-Ashchepkov

Acknowledgements

We are grateful to the stuff of electronic laboratory of the IGM SB RAS.

Conflicts of Interest

The authors declare no conflict of interest.

References

1. Kostrovitsky SI, Morikiyo T, Serov IV, Yakovlev DA, Amirzhanov AA, et al. (2007) Isotope-geochemical systematics of kimberlites and related rocks from the Siberian Platform. Russian Geology and Geophysics

48(3): 272-290.

2. Sobolev V, Sobolev AV, Tomilenko AA, Kuz'min DV, Grakhanov SA, et al. (2018) Prospects of search for diamondiferous kimberlites in the northeastern Siberian Platform. Russian Geology and Geophysics 59(10): 1365-1379.

3. Sun J, Liu CZ, Tappe S, Kostrovitsky S, Yang JH, et al. (2014) Repeated kimberlite magmatism beneath Yakutia and its relationship to Siberian flood volcanism: Insights from in situ U–Pb and Sr–Nd perovskite isotope analysis. Earth and Planetary Science Letters 404: 283-295.

4. Sun J, Tappe S, Kostrovitsky SI, Liu CZ, Skuzovatov S, et al. (2018) Mantle sources of kimberlites through time: A U-Pb and Lu-Hf isotope study of zircon megacrysts from the Siberian diamond fields. Chemical Geology 479: 228-240.

5. Zaitsev AI, Smelov AP (2010) Isotopic geochronology of rocks of the kimberlite formation of the Yakut province. Institute of diamond and precious metals Geology SB RAS, Russia, pp: 105.

6. Ukhanov AV, Khachatryan GK (2011) Diamonds from the Poiskovaya, Zapolyarnaya, and Leningrad Kimberlite Pipes, Northern Yakutia: Correlation of CarbonIsotopic Composition and Nitrogen Content As an Indicator of Fluid Diamond Formation. Geology of Ore Deposits 53(8): 783-791.

7. Kornilova VP, Spetsius ZV, Pomazanskiy BS (2016) Petrographic-mineralogical peculiarities and feasibility of kimberlite pipes Lorik and Svetlana diamond grade re-estimation (West Ukukit field, Yakutia). Regional geology and metallogeny 68: 92-99.

8. Afanasyev VP, Agashev AM, Orihashi Y, Pokhilenko NP, Sobolev NV, et al. (2009) Paleozoic U–Pb Age of Rutile Inclusions in Diamonds of the V–VII Variety from Placers of the Northeast Siberian Platform. Doklady Earth Sciences 428: 1151-1115.

9. Khmel'kov AM (2008) Major minerals of kimberlites and evolution in the process of creation of their lateral areals (example, the Yakutian diamondiferous province). ART, Novosibirsk, Russia, pp: 252.

10. Ashchepkov IV, Logvinova AM, Reimers LF, Ntaflos T, Spetsius ZV, et al. (2015) The Sytykanskaya kimberlite pipe: Evidence from deep-seated xenoliths and xenocrysts for the evolution of the mantle beneath Alakit, Yakutia, Russia. Geoscience Frontiers 6(5): 687-714.

11. Ashchepkov IV, Logvinova AM, Ntaflos T, Medvedev NS, Downes H, et al. (2017) Alakit and Daldyn kimberlite fields, Siberia, Russia: Two types of mantle sub-terranes beneath central Yakutia. Geoscience Frontiers 8(4): 671-692.

12. Ashchepkov IV, Ntaflos T, Kuligin SS, Malygina EV, Agashev AM, et al. (2013) Deep-Seated Xenoliths from the Brown Breccia of the Udachnaya Pipe, Siberia. Pearson DG, et al. (Eds.), Proceedings of 10th International Kimberlite Conference. Springer, India, pp: 59-74.

13. Ashchepkov IV, Medvedev N, Ivanov A, Vladykin N, Ntaflos T, et al. (2021) Deep mantle roots of the Zarnitsa kimberlite pipe, Siberian craton, Russia: Evidence for multistage polybaric interaction with mantle melts. Journal of Asian Earth Sciences 213: 104756.

14. Solov'eva LV, Kalashnikova TV, Kostrovitsky SI, Ivanov AV, Matsuk SS, et al. (2017) Phlogopite and phlogopite–amphibole parageneses in the lithospheric mantle of the Birekte terrane (Siberian craton). Dokl Earth Sc 475: 822-827.

15. Sun J, Rudnick RL, Kostrovitsky S, Kalashnikova T, Kitajima K, et al. (2020) The origin of low-MgO eclogite xenoliths from Obnazhennaya kimberlite, Siberian craton. Contrib Mineral Petrol 175: 25.

16. Ashchepkov IV, Kuligin SS, Vladykin NV, Downes H, Vavilov MA, et al. (2016) Comparison of mantle lithosphere beneath early Triassic kimberlite fields in Siberian craton reconstructed from deep-seated xenocrysts. Geosci Front 7(4): 639-662.

17. Dawson JB, Smith JV (1982) Upper-mantle amphiboles: a review. Mineralogical Magazine 45(337): 35-46.

18. Ridolfi F, Renzulli A (2012) Calcic amphiboles in calc-alkaline and alkaline magmas: thermobarometric and chemometric empirical equations valid up to 1,130°C and 2.2 GPa. Contrib Mineral Petrol 163: 877-895.

19. Putirka K (2016) Amphibole thermometers and barometers for igneous systems and some implications for eruption mechanisms of felsic magmas at arc volcanoes. American Mineralogist 101(4): 841-858.

20. Simakin AG, Shaposhnikova O (2017) Novel amphibole geobarometer for high-magnesium andesite and basalt magmas. Petrology 25: 226-240.

21. Niida K, Green DH (1999) Stability and chemical composition of pargasitic amphibole in MORB pyrolite under upper mantle conditions. Contrib Mineral Petrol

135: 18-40.

22. Pirard C, Hermann J (2015) Experimentally determined stability of alkali amphibole in metasomatised dunite at sub-arc pressures. Contrib Mineral Petrol 169: 1.

23. Konzett J, Sweeney R, Thompson AB, Ulmer P (1997) Potassium amphibole stability in the upper mantle: an experimental study in a peralkaline KNCMASH system to 8.5 GPa. J Petrol 38 (5): 537-568.

24. Comboni D, Lotti P, Gatta GD, Merlini M, Liermann HP, et al. (2018) Pargasite at high pressure and temperature. Physics and Chemistry of Minerals 45: 259-278.

25. Fabriès J, Lorand JP, Guiraud M (2001) Petrogenesis of the amphibole-rich veins from the Lherz orogenic lherzolite massif (Eastern Pyrenees, France): a case study for the origin of orthopyroxene-bearing amphibole pyroxenites in the lithospheric mantle. Contrib Mineral Petrol 140: 383-403.

26. Marocchi M, Hermann J, Tropper P, Bargossi GM, Mair V, et al. (2010) Amphibole and phlogopite in "hybrid" metasomatic bands monitor trace element transfer at the interface between felsic and ultramafic rocks (Eastern Alps, Italy). Lithos 117: 135-148.

27. Tedonkenfack SST, Puziewicz J, Aulbach S, Ntaflos T, Kaczmarek MA, et al. (2021) Lithospheric mantle refertilization by DMM-derived melts beneath the Cameroon Volcanic Line-a case study of the Befang xenolith suite (Oku Volcanic Group, Cameroon). Contrib Mineral Petrol 176: 37.

28. Matusiak-Malek M, Puziewicz J, Ntaflos T, Grégoire M, Kukula A, et al. (2017) Origin and evolution of rare amphibole-bearing mantle peridotites from WilczaGóra (SW Poland), Central Europe. Lithos 286-287: 302-323.

29. Giuliani A, Fiorentini ML, Martin LAJ, Farquhar J, Phillips D, et al. (2016) Sulfur isotope composition of metasomatised mantle xenoliths from the Bultfontein kimberlite (Kimberley, South Africa): contribution from subducted sediments and the effect of sulfide alteration on S isotope systematics. Earth Planet Sci Lett 445: 114-124.

30. Babushkina SA (2018) Mantle phlogopites from Leningrad pipe (from Breccia with a Massive Texture) Vestnik of the NEFU. Earth Science series 4(12): 14-19.

31. Ashchepkov I, Babushkina S, Oleinikov O, Medvedev N (2021) Unique amphibole-rich mantle beneath the Leningrad kimberlite pipe, West Ukukit field, NE Yakutia. Goldschmidt 1: 2021120444.

32. Bulanova GP, Barashkov P, Tal'nikova SB, Smelova GB (1993) Prirodnyi almaz-geneticheskie aspekty (Natural Diamond: Genetic Aspects). Nauka, Novosibirsk, Russia, pp: 215.

33. Skuzovatov SY, Shatsky VS, Wang Q, Ragozin AL, Kostrovitsky SI, et al. (2021) Multiple tectonomagmatic reactivation of the unexposed basement in the northern Siberian craton: from Paleoproterozoic orogeny to Phanerozoic kimberlite magmatism. International Geology Review 64: 1119-1138.

34. Ashchepkov IV, Vladykin NV, Kalashnyk HA, Medvedev NS, Saprykin AI, et al. (2020) Incompatible element-enriched mantle lithosphere beneath kimberlitic pipes in Priazovie, Ukrainian shield: volatile-enriched focused melt flow and connection to mature crust. International Geology Review 63(10): 1-22.

35. Shumlyanskyy LV, Kamenetsky VS, Tsymbal SM, Wilde SA, Nemchin AA, et al. (2021) Zircon megacrysts from Devonian kimberlites of the Azov Domain, Eastern part of the Ukrainian Shield: Implications for the origin and evolution of kimberlite melts. Lithos 406-407: 106528.

36. Tsymbal SN, Kremenetsky AA, Sobolev VB, Tsymbal YS (2011) Zirconium minerals from kimberlites of Novolaspinskaya pipe and dike (south-east of the Ukrainian shield). Mineralogical Journal 33: 41-62.

37. Lavrent'ev YG, Korolyuk V, Usova L, Nigmatulina E (2015) Electron probe microanalysis of rock-forming minerals with a JXA-8100 electron probe microanalyzer. Russian Geology and Geophysics 56(10): 1428-1436.

38. Lavrent'ev YG, Karmanov NS, Usova LV (2015) Electron probe microanalysis of minerals: microanalyzer or scanning electron microscope. Russian Geology and Geophysics 56(8): 1154-1161.

39. Ashchepkov IV, Andre L, Downes H, Belyatsky BA (2011) Pyroxenites and megacrysts from Vitim picrite-basalts (Russia): Polybaric fractionation of rising melts in the mantle. Journal of Asian Earth Sciences 42(1-2): 14-37.

40. Travin AV, Yudin DS, Vladimirov AG, Khromykh SV, Volkova NI, et al. (2009) Thermochronology of the Chernorud granulite zone, Ol'khon Region, Western Baikal area. Geochemistry International 47(11): 1107-1124.

41. Pokhilenko LN, Alifirova TA, Yudin DS (2013) 40Ar/39Ar-dating of phlogopite from mantle xenoliths: Evidence for deep ancient metasomatism of the Siberian craton lithosphere. Dokl Earth Sc 449: 309-312.

42. Yuan Y, Zong K, Cawood PA, Cheng H, Yu Y, et al. (2019) Implication of Mesoproterozoic (~ 1.4 Ga) magmatism within microcontinents along the southern Central Asian Orogenic Belt. Precambrian Research 327: 314-326.Malyshev SV, Ivanov AV, Khudoley AK, Marfin AE, Kamenetsky VS, et al. (2021) Global implication of mesoproterozoic (~ 1.4 Ga) magmatism within the Sette-Daban Range (Southeast Siberia). Scientific Reports 11(1): 1-10.

43. Sobolev NV, Lavrentev YG, Pokhilenko NP, Usova LV (1973) Chrome-Rich Garnets from the Kimberlites of Yakutia and Their Parageneses. Contributions to Mineralogy and Petrology 40: 39-52.

44. Dawson J B (1980) Kimberlites and their xenoliths. Springer, Berlin, Germany, pp: 252.

45. Leake BE, Woolley AR, Arps CES, Birch WD (1997) Nomenclature of amphiboles: Report of the subcommittee on amphiboles of the international association, commission on new minerals and mineral names. American Mineralogist 82: 1019-1037.

46. Locock LJ (2014) An Excel spreadsheet to classify chemical analyses of amphiboles following the IMA recommendations. Computers & Geosciences 62: 1-11.

47. Wyatt BA, Baumgartner M, Anckar E, Grutter H (2004) Compositional classification of "kimberlitic" and "non-kimberlitic" ilmenite. Lithos 77(1-4): 819-840.

48. Ashchepkov IV, Alymova NV, Logvinova AM, Vladykin NV, Kuligin SS, et al. (2014) Picroilmenites in Yakutian kimberlites: variations and genetic models. Solid Earth 5: 915-938.

49. Ashchepkov IV, Ntaflos T, Logvinova AM, Spetsius ZV, Downes H, et al. (2017) Monomineral universal clinopyroxene and garnet barometers for peridotitic, eclogitic and basaltic systems. Geoscience Frontiers 8(4): 775-795.

50. Ashchepkov IV (2006) Empirical garnet thermobarometer for mantle peridotites. Russ Geol Geophys 47(10): 1071-1085.

51. Ashchepkov IV, Pokhilenko NP, Vladykin NV, Logvinova AM, Kostrovitsky SI, et al. (2010) Structure and evolution of the lithospheric mantle beneath Siberian craton, thermobarometric study. Tectonophysics 485(1-4): 17-41.

52. Taylor WR, Kammerman M, Hamilton R (1998) New thermometer and oxygen fugacity sensor calibrations for ilmenite and chromium spinel-bearing peridotitic assemblages. 7th International Kimberlite Conference. Extended abstracts, Cape Town 7: 891-901.

53. Gudmundsson G, Wood BJ (1995) Experimental tests of garnet peridotite oxygen barometry. Contributions to Mineralogy and Petrology 119: 56-67.

54. Ashchepkov IV, Rotman AY, Somov SV, Afanasiev VP, Downes H (2012) Composition and thermal structure of the lithospheric mantle beneath kimberlite pipes from the Catoca cluster, Angola. Tectonophysics 530: 128-151.

55. Ashchepkov IV (2011) Program of the mantle thermometers and barometers: usage for reconstructions and calibration of PT methods. Vestnik Otdelenia nauk o Zemle RAN 3: NZ6008

56. Ashchepkov I (2017) Universal single grain amphibole thermobarometer for mantle rocks-preliminary calibration. EGU General Assembly Conference Abstracts, pp: 3889

57. Ravna EK (2000) Distribution of Fe2+ and Mg between coexisting garnet and hornblende in synthetic and natural systems: an empirical calibration of the garnet-hornblende Fe-Mg geothermometer. Lithos 53(3-4): 265-277

58. Brey GP, Kohler T (1990) Geothermobarometry in four-phase lherzolites. II. New thermobarometers, and practical assessment of existing thermobarometers. J Petrol 31(6): 1353-1378.

59. McGregor ID (1974) The system MgO-SiO2-Al2O3: solubility of Al2O3 in enstatite for spinel and garnet peridotite compositions. Am Miner 59: 110-119.

60. Nimis P, Taylor W (2000) Single clinopyroxene thermobarometry for garnet peridotites. Part I. Calibration and testing of a Cr-in-Cpx barometer and an enstatite-in-Cpx thermometer. Contributions to Mineralogy and Petrology 139: 541-554.

61. O'Neill HC, Wood BJ (1979) An experimental study of Fe-Mg- partitioning between garnet and olivine and its calibration as a geothermometer. Contributions to Mineralogy and Petrology 70: 59-70.

62. O'Neill HC, Wall VJ (1987) The olivine orthopyroxene-spinel oxygen geobarometer, the nickel precipitation curve, and the oxygen fugacity of the Earth's upper mantle. Journal of Petrology 28(6): 1169-1191.

63. Krogh EJ (1988) The garnet-clinopyroxene Fe-Mg geothermometer-a reinterpretation of existing experimental data. Contrib Mineral Petrol 99: 44-48.

64. Kennedy CS, Kennedy GC (1976) The equilibrium boundary between graphite and diamond. J Geophys Res 81(14): 2467-2470.

65. Day HW (2012) A revised diamond-graphite transition curve. American Mineralogist 97(1): 52-65.

66. Pollack HN, Chapman DS (1977) On the regional variation of heat flow, geotherms and lithospheric thickness. Tectonophysics 38(3): 279-296.

67. Stagno V, Frost DJ (2010) Carbon speciation in the asthenosphere: experimental measurements of the redox conditions at which carbonate - bearing melts coexist with graphite or diamond in peridotite assemblages. Earth Planet Sci Lett 300(1-2): 72-84.

68. Stagno V, Ojwang DO, McCammon CA, Frost DJ (2013) The oxidation state of the mantle and the extraction of carbon from Earth's interior. Nature 493(7430): 84-88.

69. Ashchepkov IV, Logvinova AM, Spetius ZV (2021) Thermobarometry of Inclusions: Implications to the Structure of Lithospheric Mantle and Evolution in Time and Diamond Formation. Acta Geologica Sinica-English Edition 95(S1): 18-21.

70. McCammon CA, Griffin WL, Shee SR, O'Neill HSC (2001) Oxidation during metasomatism in ultramafic xenoliths from the Wesselton kimberlite, South Africa: implications for the survival of diamond. Contrib Mineral Petrol 141: 287-296.

71. Ashchepkov IV, Vladykin NN, Ntaflos T, Kostrovitsky SI, Prokopiev SA, et al. (2014) Layering of the lithospheric mantle beneath the Siberian Craton: Modeling using thermobarometry of mantle xenolith and xenocrysts. Tectonophysics 634: 55-75.

72. Evensen NM, Hamilton PJ, Onions RK (1979) Rare-earth abundances in chondritic meteorites. Geochimica et Cosmochimica Acta 42(8): 1199-1212.

73. McDonough WF, Sun SS (1995) The composition of the Earth. Chemical Geology 120(3-4): 223-253.

74. Griffin WL, O'Reilly SY, Abe N, Aulbach S, Davies RM, et al. (2003) The origin and evolution of the Archean lithospheric mantle. Precambrian Research 127(1-3): 19-41.

75. Sobolev NV (1947) Deep-Seated Inclusions in Kimberlites and the Problem of the Composition of the Mantle. Amer Geophys Union, Washington, DC, pp: 279.

76. Pokhilenko NP, Sobolev NV, Agashev AM, Vavilov MA, Pokhilenko LN, et al. (2002) Anomalous kimberlites of the Snap Lake Area, Canada, and Nakyn Field, Yakutia: evidence of abnormal character of mantle sources and lithosphere structure. Experiment in Geosciences 10: 143-146.

77. Shatsky VS, Zedgenizov DA, Ragozin AL, Kalinina VV (2015) Diamondiferous subcontinental lithospheric mantle of the northeastern Si-berian Craton: Evidence from mineral inclusions in alluvial diamonds. Gondwana Research 28(1): 106-120.

78. Grakhanov SA, Malanin YA, Pavlov VI, Afanas'ev VP, Pokhilenko NP (2010) Rhaetian diamond placers in Siberia Russian Geology and Geophysics 51(1): 127-135.

79. Grakhanov A S, Zarubin R A, Bogush I N, Yadrenkin A B (2009) discovery of upper Triassic diamond Placers in the Olenek Bay of the Laptev sea. Otechestvennaya Geologia № 1: 53-61.

80. Dawson JB, Smith JV (1977) The MARID (mica-amphibole-rutile-ilmenite-diopside) suite of xenoliths in kimberlite. Geochim Cosmochim Acta 41(2): 309-323.

81. Banerjee S, Kyser TK, Mitchel RH (2018) Oxygen and hydrogen isotopic composition of phlogopites and amphiboles in diamond-bearing kimberlite hosted MARID xenoliths: Constraints on fluid-rock interaction and recycled crustal material in the deep continental lithospheric mantle. Chemical Geology 47920: 272-285.

82. Fitzpayne A, Giuliani A, Hergt J, Phillips D, Janney P (2018) New geochemical constraints on the origins of MARID and PIC rocks: implications for mantle metasomatism and alkaline magmatism. Lithos 318-319: 478-493.

83. Simon NSC, Carlson RW, Pearson DG, Davies GR (2007) The origin and evolution of the Kaapvaal cratonic lithospheric mantle. Journal of Petrology 48(3): 589-625.

84. Franz L, Brey GP, Okrusch M (1996) Steady state geotherm, thermal disturbances and tectonic development of the lithosphere underneath the Gibeon Kimberlite Province (Namibia). Contributions to Mineralogy Petrology 126: 181-198.

85. Franz L, Brey GP, Okrusch M (1996) Reequilibration of ultramafic xenoliths from Namibia by metasomatic processes at the mantle boundary. Journal of Geology 104 (5): 99-615.

86. Riches AJV, Ickerta RB, Pearson DG, Stern RA, Jackson SE,

et al. (2016) In situ oxygen-isotope, major-, and trace-element constraints on the metasomatic modification and crustal origin of a diamondiferous eclogite from Roberts Victor, Kaapvaalcraton Geochim Cosmochim. Acta 174: 345-359.

87. Ashchepkov IV (1991) Deep-seated xenoliths of the Baikal rift. Nauka Novosibirsk pp: 210.

88. Hutchison R, Williams CT, Henderson P, Reed SJB (1986) New varieties of mantle xenolith from the Massif Central, France. Mineral. Magazin 50: 559-565.

89. Mayer B, Jung S, Romer RL, Pfänder JA, Klügel A (2014) Amphibole in alkaline basalts from intraplate settings: implications for the petrogenesis of alkaline lavas from the metasomatised lithospheric mantle. Contribution to Mineralogy and Petrology 167(3): 988-989.

90. Coltorti M, Beccaluvam L, Bonadiman C, Faccini B, Ntaflos T (2004) Amphibole genesis via metasomatic reaction with clinopyroxene in mantle xenoliths from Victoria Land, Antarctica. Lithos 75(1): 115-139.

91. Gentili S, Bonadiman C, Biagioni C, Comodi P, Coltorti M (2015) Oxo-amphiboles in mantle xenoliths: evidence for H2O-rich melt interacting with the lithospheric mantle of Harrow Peaks Northern Victoria Land, Antarctica). Mineralogy and Petrology 109(6): 741-759.

92. Li J, Zhang S (2002) Redox state of amphibole-bearing mantle peridotite from Nushan, Anhui Province in eastern China and its implications. Sci China (Series D) 45: 348-357.

93. Ionov DA, Bénard A, Plechov P Yu, Shcherbakov VD (2013) Along-arc variations in lithospheric mantle compositions in Kamchatka, Russia: First trace element data on mantle xenoliths from the Klyuchevskoy Group volcanoes. Journal of Volcanology and Geothermal Research 263: 122-131.

94. Ionov DA, Hofmann AW (1995) Nb-Ta-rich mantle amphiboles and micas: implications for subduction-related metasomatic trace element fractionations. Earth Planet Sci Lett 131(3-4): 341-356.

95. Foley S (1991) High-pressure stability of the fluor- and hydroxy-endmembers of pargasite and K-richterite. Geochimica et Cosmochimica Acta 55(9): 2689-2694.

96. Dalpé C, Baker DR (2000) Experimental investigation of large-ion-lithophile-element-, high-field-strength-element- and rare-earth-element-partitioning between calcic amphibole and basaltic melt: the effects of pressure and oxygen fugacity. Contrib Mineral Petrol 140(2): 233-250.

97. Zhang B, Hu H, Li P, Tang O, Zhou W (2019) Trace element partitioning between amphibole and hydrous silicate glasses at 0.6–2.6 GPa. Acta Geochimica 38(3): 414-429.

98. La Tourrette T, Hervig RL, Holloway JR (1995) Trace element partitioning between amphibole, phlogopite, and basanite melt. Earth Planet. Sci Lett 135(1-4): 13-30.

99. Foley S, Tiepolo M, Vannucci R (2002) Growth of early continental crust controlled by melting of amphibolite in subduction zones. Nature 417: 837-840.

100. Faccini B, Rizzo A, Bonadiman C, Ntaflos T, Seghedi I, et al. (2020) Subduction-related melt refertilisation and alkaline metasomatism in the Eastern Transylvanian Basin lithospheric mantle: Evidence from mineral chemistry and noble gases in fluid inclusions. Lithos 364-365: 105516.

101. Fumagalli P, Poli S (2005) Experimentally determined phase relations in hydrous peridotites to 6.5 GPa and their consequences on the dynamics of subduction zones. J Petrology 46(3): 555-578.

102. Ashchepkov IV, Vladykin NV, Ntaflos T, Downes H, Mitchel R, et al. (2013) Regularities of the mantle lithosphere structure and formation beneath Siberian craton in comparison with other cratons. Gondwana Research 23(1): 4-24.

103. Rosenthal A, Yaxley GM, Green DH, Hermann J (2014) Continuous eclogite melting and variable refertilisation in upwelling heterogeneous mantle. Scientific Reports 4: 6099.

104. Rosenthal A, Hauri EH, Hirschmann MM (2016) Experimental determination of C, F and H partitioning between mantle minerals and carbonated basalt, CO2/Ba and CO2/Nb systematics of partial melting, and the CO2 contents of basaltic source regions. Earth Planet Sci Lett 412: 77-87.

105. Ionov DA, Doucet LS, Ashchepkov IV (2010) Composition of the Lithospheric Mantle in the Siberian Craton: New Constraints from Fresh Peridotites in the Udachnaya-East Kimberlite. Journal of Petrology 51(11): 2177-2210.

106. Pernet-Fisher JF, Howarth JH, Pearson DG, Woodland S, Barry PH, et al. (2015) Plume impingement on the Siberian SCLM: evidence from Re–Os isotope

systematics. Lithos 218-219: 141-154.

107. Cull JP, O'Reilly SY, Griffin WL (1991) Xenolith geotherms and crustal models in Eastern Australia. Tectonophysics 192(3-4): 359-366.

108. Manning CE (2004) The chemistry of subduction-zone fluids. Earth Planet Sci Lett 223(1-2): 1-16.

109. Foley SF, Barth MG, Jenner GA (2000) Rutile/melt partition coefficients for trace elements and an assessment of the influence of rutile on the trace element characteristics of subduction zone magmas. Geochimica et Cosmochimica Acta 64(5): 933-938.

110. Bedard JH (2006) A catalytic delamination-driven model for coupled genesis of Archaean crust and sub-continental lithospheric mantle. Geochimica et Cosmochimica Acta 70(5): 1188-1214.

111. Gregoire M, Bell DR, Le Roex AP (2003) Garnet Lherzolites from the Kaapvaal Craton (South Africa): trace element evidence for a metasomatic history. J Petrol 44(4): 629-657.

112. Chen Y, Niu Y, Xue Q, Gao Y, Castillo P (2021) An iron isotope perspective on back-arc basin development: Messages from Mariana Trough basalts. Earth and Planetary Science Letters 572: 117133.

113. Kent AJR, Elliott T (2002) Melt inclusions from Marianas arc lavas: implications for the composition and formation of island arc magmas. Chemical Geology 183(1-4): 263-286.

114. Carter EJ, O'Driscoll B, Burgess R, Clay PL (2021) Multi-stage fluid infiltration and metasomatism in supra-subduction zone mantle: evidence from halogens and noble gases in the Leka Ophiolite Complex, Norway. Geochimica et Cosmochimica Acta 307: 258-280.

115. Bénard A, Koga KT, Shimizu N, Kendrick MA, Ionov DA, et al. (2017) Chlorine and fluorine partition coefficients and abundances in sub-arc mantle xenoliths (Kamchatka, Russia): Implications for melt generation and volatile recycling processes in subduction zones. Geochimica et Cosmochimica Acta 199: 324-350.

116. Wang D, Romer RL, Guo JH, Glodny G (2020) Li and B isotopic fingerprint of Archean subduction. Geochimica et Cosmochimica Acta 268: 446-466.

117. Song S, Niu Y, Su L, Wei C, Zhang L (2014) Adakitic (tonalitic-trondhjemitic) magmas resulting from eclogite decompression and dehydration melting during exhumation in response to continental collision. Geochimica et Cosmochimica Acta 130: 42-62.

118. Smart KA, Tappe S, Woodland AB, Harris C, Corcoran L, et al. (2021) Metasomatized eclogite xenoliths from the central Kaapvaal craton as probes of a seismic mid-lithospheric discontinuity. Chemical Geology 578: 120286.

119. Boettcher AL, O'Neil JR (1980) Stable isotope, chemical, and petrographic studies of high-pressure amphiboles and micas: evidence for metasomatism in the mantle source regions of alkali basalts and kimberlites. Am J Sci 280: 594-621.

120. Ashchepkov I, Logvinova A, Spetsius Z, Downes H, Ntaflos T, et al. (2022) Eclogite Varieties and Their Positions in the Cratonic Mantle Lithosphere beneath Siberian Craton and Archean Cratons Worldwide. Minerals 12(11): 1353.

121. Dawson JB, Smith JV (1982) Upper-mantle amphiboles: a review. Mineralogical Magazine 45(337): 35-46.

122. Ernst WG, Liu J (1998) Experimental phase-equilibrium study of Al- and Ti-contents of calcic amphibole in MORB – A semiquantitative thermobarometer. American Mineralogist 83(9-10): 952-969.

123. Popp RK, Hibbert HA, Lamb WM (2006) Oxy-amphibole equilibria in Ti-bearing calcic amphiboles: experimental investigation and petrologic implications for mantle-derived amphiboles. Am Mineral 91(1): 54-66.

124. Konzett J, Krenn K, Rubatto D, Hauzenberger C, Stalder R (2014) The formation of saline mantle fluids by open-system crystallization of hydrous silicate-rich vein assemblages – evidence from fluid inclusions and their host phases in MARID xenoliths from the central Kaapvaal Craton, South Africa. Geochim Cosmochim Acta 147: 1-25.

125. Medard E, Schmidt MW, Schiano P, Ottolini L (2006) Melting of Amphibole-bearing Wehrlites: an Experimental Study on the Origin of Ultra-calcic Nepheline-normative Melts. Journal of Petrology 47(3): 481-504.

126. Foley S (1992) Vein-plus-wall-rock melting mechanisms in the lithosphere and the origin of potassic alkaline magmas. Lithos 28(3-6): 435-453.

127. Schmidt MW (1992) Amphibole composition in tonalite as a function of pressure: an experimental calibration of the Al-in-hornblende barometer. Contrib Mineral Petrol 110: 304-310.

128. Schmidt MW, Dardon A, Chazot G, Vannucci R (2004) The dependence of Nb and Ta rutile–melt partitioning

on melt composition and Nb/Ta fractionation during subduction processes. Earth and Planetary Science Letters 226(3-4): 415-432.

129. Sun C, Dasgupta R (2019) Slab–mantle interaction, carbon transport, and kimberlite generation in the deep upper mantle. Earth and Planetary Science Letters 506: 38-52.

130. Trønne RG (2002) Stability range and decomposition of potassic richterite and phlogopite end members at 5-15 GPa. Mineralogy and Petrology 74: 129-148.

131. Ridolfi F, Renzulli A, Puerini M (2010) Stability and chemical equilibrium of amphibole in calc-alkaline magmas: an overview, new thermobarometric formulations and application to subduction-related volcanoes. Contrib Mineral Petrol 160: 45-66.

132. Wallace ME, Green DH (1991) The effect of bulk rock composition on the stability of amphibole in the upper mantle: implications for solidus positions and mantle metasomatism. Mineral Petrol 44: 1-19.

133. Wyllie PJ (1978) Mantle fluid compositions buffered in peridotite-CO2-H2O by carbonates, amphiboles and phlogopite. J Geol 86(6): 687-713.

134. Hunt L, Stachel T, McCandless TE, Armstrong J, Muelenbachs K (2012) Diamonds and their mineral inclusions from the Renard kimberlites in Quebec. Lithos 142-143: 267-284.

135. Waters FG, Erlank AJ, Daniels L (1989) Contact relationships between MARID rock and metasomatised peridotite in a kimberlite xenolith. Geochemical Journal 23(1): 11-17.

136. Konzett J, Armstrong RA, Sweeney RJ, Compston W (1998) The timing of MARID metasomatism in the Kaapvaal mantle: An ion probe study of zircons from MARID xenoliths. Earth and Planetary Science Letters 160(1-2): 133-145.

137. Pearson DG, Shirey SB, Carlson RW, Boyd FR, Pokhilenko NP, et al. (1995) Re–Os, Sm–Nd and Rb–Sr isotope evidence for thick Archaean lithospheric mantle beneath the Siberia craton modified by multi-stage metasomatism. Geochim Cosmochim Acta 59(5): 959-977.

138. Griffin WL, Ryan CG, Kaminsky FV, O'Reilly SY, Natapov LM, et al. (1999) The Siberian lithosphere traverse: mantle terranes and the assembly of the Siberian Craton. Tectonophysics 310(1-4): 1-35.

139. Griffin WL, Natapov LM, O'Reilly SY, van Achterbergh E, Cherenkova AF, et al. (2005) The Kharamai kimber-lite field, Siberia: modification of the lithospheric mantle by the Siberian Trap event. Lithos 81(1-4): 167-187.

Appendix A. Amphibole Thermobarometer Equations

Barometer
XFe3am=Fe+Mn+Mg+Ca-4; xAMKd=Si**1/(Al+XFe3am+2*Ti))**0.75*(Na+K))/Ca;
P=0.0575*(4+(K/(Na+K)*1.5*Mg)/Fe+4.25*(0.85*Na+1.10*K)/Ca))*xaMkD*ToK**0.75/(1+7*Fe)-Ln(1273/(ToK))*2.5*(3.8*Mg-Al*2.3)+3*Ti)!+12*Cr+2*K)+25-0.04*Ti*ToK-Ca*(ToK-750)/300; P=P*0.9+5+1.55*Ti

Thermometer. Ravna, 2000 Gar-Amphibole (monomineral version)
CaGar= 0.1958*CaAm+0.1889; MgGar = 0.475* MgAm-0.5753+0.0035*P; FeGar = 1.125* FeAm-0.1132-0.0001*P
Z =Ca+Fe+Mg ; FeGar=FeGar*3/Z; MgGar = MgGar *3/Zl CaGar = CaGar*3/Z; x581=Ca/3; x561=Mn/3xKD= (Fe/Mg) *Gar**(Mg/Fe)$_{Am}$
T=(1504+1784*(x581+x561))/(Ln(xKD)+0.720)
Corrections: T=T-(52-SiO2))*35+50+5*Ti; T=T+(P-50)*2.5-20
Where P – pressure in kbar; T – ToK.
The method is realized in the PT program written in FORTRAN 77 [55].
The results of the calibration and the correlations of the calculations with the experimental values are represented on the diagram (Figure 10).